

Dynamical coupled-channel approach to hadronic and electromagnetic production of kaon-hyperon on the proton

B. Juliá-Díaz,^{1,*} B. Saghai,^{1,†} T.-S. H. Lee,^{2,‡} and F. Tabakin^{3,§}

¹*Laboratoire de recherche sur les lois fondamentales de l'Univers,
DSM/Dapnia, CEA/Saclay, 91191 Gif-sur-Yvette, France*

²*Physics Division, Argonne National Laboratory, Argonne, IL 60439, USA*

³*Department of Physics and Astronomy, University of Pittsburgh, USA*

(Dated: July 12, 2018)

Abstract

A dynamical coupled-channel formalism for processes $\pi N \rightarrow KY$ and $\gamma N \rightarrow KY$ is presented which provides a comprehensive investigation of recent data on the $\gamma p \rightarrow K^+\Lambda$ reaction. The non-resonant interactions within the subspace $KY \oplus \pi N$ are derived from effective Lagrangians, using a unitary transformation method. The calculations of photoproduction amplitudes are simplified by casting the coupled-channel equations into a form such that the empirical $\gamma N \rightarrow \pi N$ amplitudes are input and only the parameters associated with the KY channel are determined by performing χ^2 -fits to all of the available data for $\pi^- p \rightarrow K^0\Lambda$, $K^0\Sigma^0$ and $\gamma p \rightarrow K^+\Lambda$. Good agreement between our models and those data are obtained. In the fits to $\pi N \rightarrow KY$ channels, most of the parameters are constrained within $\pm 20\%$ of the values given by the Particle Data Group and/or quark model predictions, while for $\gamma p \rightarrow K^+\Lambda$ parameters, ranges compatible with broken $SU(6) \otimes O(3)$ symmetry are imposed. The main reaction mechanisms in $K^+\Lambda$ photoproduction are singled out and issues related to newly suggested resonances S_{11} , P_{13} , and D_{13} are studied. Results illustrating the importance of using a coupled-channel treatment are reported. Meson cloud effects on the $\gamma N \rightarrow N^*$ transitions are also discussed.

PACS numbers: 11.80.-m, 11.80Gw, 13.75.-n, 24.10.Eq

*bjulia@ecm.ub.es

†bijan.saghai@cea.fr

‡lee@phy.anl.gov

§tabakin@pitt.edu

I. INTRODUCTION

Recent experiments at JLab-CLAS [1, 2], ELSA-SAPHIR [3, 4] and Spring-8-LEPS [5, 6] are refining our knowledge of associated strangeness photoproduction. High precision differential cross section data for the process $\gamma p \rightarrow K^+ \Lambda$ have been released [1, 3, 6] covering the region between $W \approx 1.6$ GeV and 2.6 GeV in the center-of-mass frame. Furthermore, single polarization asymmetry data for recoil hyperon [2] and beam [5, 6] have also become available.

The $K^+ \Lambda$ photoproduction has also been extensively studied using phenomenological approaches. In general, those works [7, 8, 9, 10, 11, 12] investigated the direct channel mechanisms based on an isobar approach in tree approximation. Combinations of isobar models with a Regge analysis [13], successful at higher energies, have also focused [14, 15] on strangeness electromagnetic production. A new generation of more precise data has made it clear that coupled-channel effects can no longer be ignored and that multi-step processes have to be incorporated carefully. Coupled-channel formalisms based on the K-matrix approximation and isobar effective Lagrangians have been developed [16, 17].

The purpose of this work is to report on an advanced version of a dynamical coupled-channel formalism [18, 19, 20, 21] that incorporates proper treatment of off-shell effects. The direct KY photoproduction channel is investigated via a chiral constituent quark model (CQM) [22, 23]. This latter approach allows one to handle all known resonances with a reasonable number of adjustable parameters, in contrast to isobar effective Lagrangian models [24]. Consequently, the CQM provides an appropriate tool for understanding the elementary reaction mechanism, establishing reliable indicia for the predicted missing baryon resonances [25, 26, 27, 28, 29, 30, 31, 32], and gaining improved insights into the known resonances.

In principle, the KY photoproduction should be investigated within a large scale coupled-channel approach including several reaction channels, e.g. πN , ηN , ωN , KY , ϕN , $\pi\pi N$ (σN , $\pi\Delta$, ρN). Obviously, this can not be done so easily because the data sets, to be simultaneously fitted, are very extensive, and reaction mechanisms involving channels other than πN have not been studied extensively.

As a first significant step, it is useful to consider a much more restricted coupled-channel model focusing on understanding particular reaction mechanisms. Concerning the KY pho-

toproduction, the obvious first task is to investigate the coupling between the KY and πN channels for the following reasons. From the available data, one observes that kaon photoproduction is in general much weaker than pion photoproduction. Hence the multi-step transitions, such as $\gamma N \rightarrow \pi N \rightarrow KY$, should be comparable to the direct $\gamma N \rightarrow KY$ process. This has been verified in Ref. [18] using a coupled-channel model with γN , πN and KY channels. Moreover, the need for a coupled-channel approach to study meson-baryon reactions in the second and third N^* regions has been well discussed in the literatures, as reviewed in Refs. [33, 34].

In this work, we take advantage of the development of new models [19] for $\pi N \rightarrow KY$ and $KY \rightarrow KY$ interactions to reinvestigate the influence of the πN channel. Furthermore, we refine the models developed in Refs. [18, 19] and consider recent $\gamma p \rightarrow K^+\Lambda$ data. Focusing on the coupled-channel effects associated with the πN channel, we also determine the parameters of relevant N^* resonances. Our results could serve as the starting point for performing more advanced coupled-channel calculations including additional meson-baryon channels.

Within the considered coupled-channel model, a comprehensive study of $K^+\Lambda$ photoproduction requires models of the non-resonant transitions among γN , πN , and KY states and the decays into these three channels for about 12 isospin $I = 1/2$ N^* states. In this work, we follow Refs. [18, 19] to derive the non-resonant transitions from effective Lagrangians by using a unitary transformation method [35] and SU(3) symmetry. For N^* decays, we consider information from the Particle Data Group [36] (PDG) and/or from constituent quark model predictions [27, 28, 29]. With these constraints, the model has a reasonable number of adjustable parameters, which can only be ascertained from the data. We simplify the fitting task by casting the coupled-channel equations into a form such that the empirical $\gamma N \rightarrow \pi N$ amplitudes [37] are input to the calculations and only the parameters associated with the KY channel are to be determined by performing χ^2 minimization fits to all available $\pi N \rightarrow KY$ and $\gamma N \rightarrow KY$ data, using the CERN-MINUIT code.

In addition, to clarify the role of coupled-channel effects due to the πN channel, we also analyze the dynamical content of the $\gamma N \rightarrow N^*$ transition. The so-called ‘‘meson cloud effects’’ discussed in the study [35, 38] of the $\Delta(1232)$ resonance are identified within our coupled-channel model. We also make an attempt to determine the properties of the predicted [26, 27, 28, 29, 30, 31, 32, 39] and/or sought for [8, 11, 14, 16, 20, 23, 40, 41, 42,

43, 44, 45, 46, 47] third S_{11} , P_{13} , and D_{13} resonances.

For simplicity, at this stage we do not consider the $K\Sigma$ photoproduction data to avoid the need to also determine the parameters associated with the photo-excitations of about 12 other isospin $I = 3/2$ N^* states. Obviously, our results serve as a good starting point for a subsequent investigation including all KY channels. Our results in that direction will be published elsewhere.

This paper is organized as follows: In Section II, the theoretical frame is presented. The main content of our coupled-channel formalism is then given, followed by an outline of the relevant constituent quark model for the direct $\gamma p \rightarrow K^+\Lambda$ channel. There, the novelties of our approach are discussed. Section III is devoted to numerical results and comparisons with available data for $\pi^-p \rightarrow K^0\Lambda$, $K^0\Sigma^0$ and $\gamma p \rightarrow K^+\Lambda$. For this latter reaction, the most relevant known nucleon resonances are singled out and possible manifestations of new baryon resonances are discussed. Meson cloud effects are exhibited by examining multipoles from the obtained model. Summary and conclusions are reported in Section IV.

II. THEORETICAL FORMULATION

In this Section, we first present our dynamical coupled-channel approach for the photoproduction process including intermediate πN and KY channels. Then, we outline the constituent quark model used for the direct KY photoproduction reaction.

A. Coupled-channel formalism

The coupled-channel approach presented here is derived from a general formulation reported in Refs. [33, 34]. The starting point is a Hamiltonian consisting of non-resonant terms $v_{a,b}$ plus resonant terms $v_{a,b}^R = \Gamma_{N^*,a}^\dagger \Gamma_{N^*,b} / (E - M_{N^*}^0)$, where a, b are the considered meson-baryon channels, $M_{N^*}^0$ is the bare mass of the N^* state, and $\Gamma_{N^*,a}$ describe the $N^* \rightarrow a$ decays. Such a Hamiltonian can be derived from effective Lagrangians using a unitary transformation method developed in Ref. [35]. By using the two potential formulation [48], as also derived explicitly in Appendix A, one can cast exactly the transition amplitude $T_{a,b}(E)$ for the $a \rightarrow b$ reaction into a sum of non-resonant $t_{a,b}(E)$ and resonant $t_{a,b}^R(E)$ terms:

$$T_{a,b}(E) = t_{a,b}(E) + t_{a,b}^R(E). \quad (1)$$

The first term of Eq. (1) is determined only by the non-resonant interactions

$$t_{a,b}(E) = v_{a,b} + \sum_c v_{a,c} G_c(E) t_{c,b}(E), \quad (2)$$

where $G_c(E)$ is the propagator of the meson-baryon state c . The resonant term is

$$t_{a,b}^R(E) = \sum_{N_i^*, N_j^*} \bar{\Gamma}_{N_i^*, a}^\dagger(E) [G^{N^*}(E)]_{i,j} \bar{\Gamma}_{N_j^*, b}(E). \quad (3)$$

The resonant amplitude in Eq. (3) is determined by the dressed vertex

$$\bar{\Gamma}_{N^*, a}(E) = \Gamma_{N^*, a} + \sum_b \Gamma_{N^*, b} G_b(E) t_{b,a}(E), \quad (4)$$

and the dressed N^* propagator

$$[G^{N^*}(E)^{-1}]_{i,j}(E) = (E - M_{N_i^*}^0) \delta_{i,j} - \Sigma_{i,j}(E). \quad (5)$$

Here the N^* self-energy is defined by

$$\Sigma_{i,j}(E) = \sum_a \bar{\Gamma}_{N_i^*, a} G_a(E) \Gamma_{N_j^*, a}^\dagger(E). \quad (6)$$

In this work, we make the following simplifications. We keep only three channels γN , KY and πN , and neglect the terms with electromagnetic coupling strengths higher than the first order e . We further assume that the N^* propagator Eq. (5) can be replaced by a simple phenomenological Breit-Wigner form. Then, Eqs. (1)-(6) are reduced to the following expressions for calculating the $\gamma N \rightarrow KY$ and $\pi N \rightarrow KY$ amplitudes:

$$T_{\gamma N, KY}(E) = t_{\gamma N, KY}(E) + \sum_{N^*} \frac{\bar{\Gamma}_{N^*, \gamma N}^\dagger \bar{\Gamma}_{N^*, KY}}{E - M_{N^*} + i\Gamma^{tot}(E)/2}, \quad (7)$$

$$T_{\pi N, KY}(E) = t_{\pi N, KY}(E) + \sum_{N^*} \frac{\bar{\Gamma}_{N^*, \pi N}^\dagger \bar{\Gamma}_{N^*, KY}}{E - M_{N^*} + i\Gamma^{tot}(E)/2}, \quad (8)$$

with

$$\bar{\Gamma}_{N^*, \gamma N}^\dagger = \Gamma_{N^*, \gamma N}^\dagger + [t_{\gamma N, KY} G_{KY} \Gamma_{N^*, KY}^\dagger + t_{\gamma N, \pi N} G_{\pi N} \Gamma_{N^*, \pi N}^\dagger], \quad (9)$$

$$\bar{\Gamma}_{N^*, \pi N}^\dagger = \Gamma_{N^*, \pi N}^\dagger + [t_{\pi N, KY} G_{KY} \Gamma_{N^*, KY}^\dagger + t_{\pi N, \pi N} G_{\pi N} \Gamma_{N^*, \pi N}^\dagger], \quad (10)$$

$$\bar{\Gamma}_{N^*, KY} = \Gamma_{N^*, KY} + [\Gamma_{N^*, KY} G_{KY} t_{KY, KY} + \Gamma_{N^*, \pi N} G_{\pi N} t_{\pi N, KY}]. \quad (11)$$

It is clear that the first step to solve the above equations is to develop models for calculating all non-resonant amplitudes. To first order in electromagnetic coupling, within the

considered $\gamma N \oplus KY \oplus \pi N$ space, Eq. (2) leads to

$$\begin{aligned} t_{\gamma N, KY} &= v_{\gamma N, KY} [1 + G_{KY}(E) t_{KY, KY}(E)] + v_{\gamma N, \pi N} G_{\pi N}(E) t_{\pi N, KY} \\ &= v_{\gamma N, KY} [1 + G_{KY}(E) t_{KY, KY}(E)] + t_{\gamma N, \pi N} G_{\pi N}(E) v_{\pi N, KY}. \end{aligned} \quad (12)$$

Here we note that the second line of the above equation is obtained from using the well-known property $vgt = tgv$. The non-resonant amplitudes $t_{KY, KY}$ and $t_{\pi N, KY}$ in Eq. (12) are obtained by solving Eq. (2) within the subspace $KY \oplus \pi N$. For numerical reasons, we follow the procedure of Ref. [18] to eliminate $t_{\pi N, \pi N}$ from these coupled equations. We then obtain the following equations

$$t_{KY, KY} = v_{KY, KY}^{\text{eff}} + \sum_{KY} v_{KY, KY}^{\text{eff}} G_{KY} t_{KY, KY}, \quad (13)$$

$$\begin{aligned} t_{KY, \pi N} &= [v_{KY, \pi N} + t_{KY, KY} G_{KY} v_{KY, \pi N}] \\ &\times [1 + G_{\pi N} \hat{t}_{\pi N, \pi N}], \end{aligned} \quad (14)$$

where

$$v_{KY, KY}^{\text{eff}} = v_{KY, KY} + \sum_{\pi N} v_{KY, \pi N} G_{\pi N} v_{\pi N, KY}^{\text{eff}}, \quad (15)$$

with

$$v_{\pi N, KY}^{\text{eff}} = v_{\pi N, KY} + \sum_{\pi N} \hat{t}_{\pi N, \pi N} G_{\pi N} v_{\pi N, KY}. \quad (16)$$

The pure πN scattering t-matrix $\hat{t}_{\pi N, \pi N}$ in the above equations is defined by

$$\hat{t}_{\pi N, \pi N} = v_{\pi N, \pi N} + v_{\pi N, \pi N} G_{\pi N} \hat{t}_{\pi N, \pi N}. \quad (17)$$

We see that Eqs. (13) and (17) are single channel integral equations. The couplings between πN and KY channels are isolated in the effective potentials $v_{KY, KY}^{\text{eff}}$ and $v_{\pi N, KY}^{\text{eff}}$. Clearly, the use of Eqs. (13)-(17) greatly simplifies the numerical task of handling the matrix problem associated with the original coupled-channel integral equations in the subspace $KY \oplus \pi N$. In fact, this technique will be useful for future investigations including additional channels.

To solve the above equations, we employ the non-resonant potentials $v_{KY, KY}$, $v_{\pi N, KY}$ derived in Ref. [19] from effective Lagrangians using a unitary transformation method of Ref. [35]. The expressions for these potentials can be found there and will not be repeated here. However, we depart from Ref. [19] in two aspects. First, Eq. (17) for determining

$\hat{t}_{\pi N, \pi N}$ was not solved directly in Ref. [19]. Instead, it was estimated from using the empirical $\pi N \rightarrow \pi N$ amplitudes. In this work, we solve Eq. (17) by using $v_{\pi N, \pi N}$ of Ref. [35] which was also derived from effective Lagrangians using the same unitary transformation method. The second new aspect of our calculations is to include the distortion effects on the N^* decays, defined by the term within the square brackets in the right-hand-side of Eqs. (10)-(11), which were neglected in the calculations of Ref. [19]. It turns out that these two refinements do not change much the quality of the fits to the $\pi N \rightarrow KY$ data. More details will be given in the next Section.

We now discuss the calculation of the non-resonant kaon photoproduction amplitude defined by Eq. (12). While the main contribution to $t_{\gamma N, KY}$ is expected to be from the direct transition amplitude $v_{\gamma N, KY}$, the calculations of the coupled-channel effects due to the πN channel require a model for the $\gamma N \rightarrow \pi N$ amplitude $t_{\gamma N, \pi N}$. The amplitude $t_{\gamma N, \pi N}$ is expected to be rather complicated in the second and third N^* regions. Full construction of $t_{\gamma N, \pi N}$ is far beyond the scope of this work. To make progress, we follow the phenomenological procedure of Ref. [49] to define $t_{\gamma N, \pi N}$ in terms of the empirical $\gamma N \rightarrow \pi N$ amplitude and the resonant amplitude constructed from the quark model predictions of Ref. [27, 28, 29]. Explicitly, we define

$$t_{\pi N, \gamma N} \equiv T_{\pi N, \gamma N}^{\text{SAID}} - t_{\pi N, \gamma N}^{\text{QM,R}}, \quad (18)$$

where $t_{\pi N, \gamma N}^{\text{QM,R}}$ is the quark model amplitude given explicitly in Ref. [49] and $T_{\pi N, \gamma N}^{\text{SAID}}$ is obtained from the 1995 solution of the SAID [37] analysis. As an alternative, we can replace $t_{\pi N, \gamma N}^{\text{QM,R}}$ by $t_{\pi N, \gamma N}^{\text{PDG,R}}$ which is the $\gamma N \rightarrow N^* \rightarrow \pi N$ amplitude defined by the resonance parameters listed by PDG. Unfortunately, the parameters of $\gamma N \rightarrow N^*$ for most of the considered N^* are not well determined by PDG. In fact, this work is one of the possible ways to learn about these $\gamma N \rightarrow N^*$ amplitudes by considering the photoproduction channels other than the πN channel. We thus use Eq. (18) in this work.

Eq. (18) only defines the on-shell values of the amplitude $t_{\pi N, \gamma N}$. For the calculation of Eq. (12), which involves integrations over off-shell matrix elements, we define the following off-shell behavior

$$t_{\pi N, \gamma N}(q, k_0, W) = t_{\pi N, \gamma N}(q_0, k_0, W) \frac{F(q, \Lambda)}{F(q_0, \Lambda)}, \quad (19)$$

with

$$F(q, \Lambda) = \left(\frac{\Lambda^2}{\Lambda^2 + q^2} \right)^2, \quad (20)$$

$$q_0 = \frac{[(W^2 - m_N^2 - m_\pi^2)^2 - 4m_N^2 m_\pi^2]^{1/2}}{2W}, \quad (21)$$

where W is the invariant mass of the πN system, q is πN off-shell momentum, k_0 is the on-shell momentum of the initial γN system, and the cutoff Λ is an adjustable parameter in our fit to the $\gamma N \rightarrow KY$ data. We find $\Lambda = 1.5$ GeV.

B. Direct channel

For the non-resonant $\gamma N \rightarrow KY$ transition amplitude $v_{\gamma N, KY}$ and the resonant amplitude, we follow the procedure of Refs. [22, 23]. The details can be found there and will not be repeated here. Below, we summarize the main points needed in the subsequent Section.

The chiral constituent quark approach is based on a low energy QCD-inspired Lagrangian [50], where the scattering matrix for the photoproduction of pseudoscalar mesons can be derived [51] as

$$\begin{aligned} \mathcal{M}_{fi} = & \langle N_f | H_{m,e} | N_i \rangle + \sum_j \left\{ \frac{\langle N_f | H_m | N_j \rangle \langle N_j | H_e | N_i \rangle}{E_i + \omega - E_j} + \frac{\langle N_f | H_e | N_j \rangle \langle N_j | H_m | N_i \rangle}{E_i - \omega_m - E_j} \right\} \\ & + \mathcal{M}_T. \end{aligned} \quad (22)$$

Here, $N_i(N_f)$ is the initial (final) state of the nucleon, $\omega(\omega_m)$ represents the energy of incoming (outgoing) photons, and H_m and H_e are pseudovector and electromagnetic couplings, respectively, and N_j is the intermediate baryon.

The first term in Eq. (22) is a seagull term. The second and third terms correspond to the s - and u -channels, respectively. The last term \mathcal{M}_T is the t -channel contribution.

The contribution from the s -channel resonances to the transition matrix elements can be written as

$$\mathcal{M}_{N^*}^{CQM} = \frac{2M_{N^*}}{W^2 - M_{N^*}(M_{N^*} - i\Gamma(q))} e^{-\frac{k^2+q^2}{6\alpha_{ho}^2}} \mathcal{A}_{N^*}, \quad (23)$$

with $k = |\mathbf{k}|$ and $q = |\mathbf{q}|$ the momenta of the incoming photon and the outgoing meson, respectively; W is the total energy of the system, $e^{-(k^2+q^2)/6\alpha_{ho}^2}$ a form factor in the harmonic oscillator basis with the parameter α_{ho}^2 related to the harmonic oscillator strength in the

wave-function, and M_{N^*} and $\Gamma(q)$ the mass and the total width of the resonance, respectively. The amplitudes \mathcal{A}_{N^*} are divided into two parts: the contribution from each resonance below 2 GeV (these transition amplitudes have been translated into the standard CGLN amplitudes in the harmonic oscillator basis), and the contributions from the resonances above 2 GeV, which are treated as degenerate [51].

The contributions from each resonance is determined by introducing [22] a new set of real parameters C_{N^*} for the amplitudes \mathcal{A}_{N^*} :

$$\mathcal{A}_{N^*} \rightarrow C_{N^*} \mathcal{A}_{N^*}, \quad (24)$$

so that

$$\mathcal{M}_{N^*}^{exp} = C_{N^*}^2 \mathcal{M}_{N^*}^{CQM}, \quad (25)$$

where $\mathcal{M}_{N^*}^{exp}$ is the experimental value of the observable, and $\mathcal{M}_{N^*}^{CQM}$ is calculated in the quark model [23]. For instance, for resonance with mass ≤ 2 GeV, the $SU(6) \otimes O(3)$ symmetry predicts $C_{N^*} = 0.0$ for $S_{11}(1650)$, $D_{13}(1700)$, and $D_{15}(1675)$ resonances, and $C_{N^*} = 1.0$ for other ones. However, deviations from those central values are anticipated within the broken $SU(6) \otimes O(3)$ symmetry, due for example to one-gluon exchange mechanisms [52].

III. RESULTS AND DISCUSSION

This Section is devoted to the application of our formalism to the production of kaon-hyperon final states in πN and γp collisions.

To that end, we need first to study $\pi N \rightarrow KY$, and $KY \rightarrow KY$ processes. In the following we first compare our $\pi N \rightarrow KY$ results with the relevant data and also extract N^* information within the considered model. Then we present results for the photoproduction channel and discuss issues related to the missing resonances.

A. $\pi N \rightarrow KY$ Reaction

As seen in Eq. (12), to calculate $\gamma N \rightarrow KY$ amplitude our first step is to construct the non-resonant amplitudes $t_{KY,KY}$ and $t_{\pi N,KY}$. These are obtained within our model by solving the coupled-channel equations (13)-(17). The input of these coupled-channel

Notation	Resonance	Coupling	Value
		$f_{K\Lambda N}$	-0.61
		$f_{K\Sigma N}$	0.12
		$f_{\pi\Sigma\Lambda}$	0.08
		$f_{\pi\Sigma\Sigma}$	0.00
$N4$	$S_{11}(1650) 1/2^-$	$f_{K\Lambda N4}$	-0.25
		$f_{K\Sigma N4}$	-0.20
$N5$	$D_{13}(1700) 3/2^-$	$f_{K\Lambda N5}$	-0.33
		$f_{K\Sigma N5}$	0.08
$N6$	$P_{11}(1710) 1/2^+$	$f_{K\Lambda N6}$	0.09
		$f_{K\Sigma N6}$	-0.32
$N7$	$P_{13}(1720) 3/2^+$	$f_{K\Lambda N7}$	-0.56
		$f_{K\Sigma N7}$	0.54
$D1$	$S_{31}(1900) 1/2^-$	$f_{K\Sigma D1}$	0.09
$D2$	$P_{31}(1910) 1/2^+$	$f_{K\Sigma D2}$	0.20
$D3$	$P_{33}(1920) 3/2^+$	$f_{K\Sigma D3}$	-0.20
$L3$	$S_{01}(1670) 1/2^-$	$f_{\pi\Sigma L3}$	-0.20
$L5$	$P_{01}(1810) 1/2^+$	$f_{\pi\Sigma L5}$	-0.01
$S1$	$P_{11}(1660) 1/2^+$	$f_{\pi\Lambda S1}$	-0.20
		$f_{\pi\Sigma S1}$	-0.20
$S4$	$D_{13}(1670) 3/2^-$	$f_{\pi\Lambda S4}$	0.22
		$f_{\pi\Sigma S4}$	0.05
	K^*NY couplings	$f_{K^*N\Lambda}^V$	0.71
		$f_{K^*N\Lambda}^T$	-3.97
		$f_{K^*N\Sigma}^V$	-0.53
		$f_{K^*N\Sigma}^T$	0.52
	cut-offs	Λ_s	623.0
		Λ_u	1468.0
		Λ_i	930.0
		$\Lambda_{\pi N}$	1491.0
	off-shell	X	2.0
	Reduced χ^2		1.86

TABLE I: Coupling constants in $\pi N \rightarrow KY$ and $KY \rightarrow KY$. The values are extracted from our minimization procedure. The parameters are defined in the model B of Ref. [19].

equations are the potentials $v_{KY,\pi N}$, $v_{KY,KY}$, and an effective non-resonant amplitude $\hat{t}_{\pi N\pi N}$ which is defined by Eq. (17). The parameters of these potentials are then adjusted along with the N^* parameters associated with the resonant term of Eq. (8) to fit the $\pi^- p \rightarrow K^0\Lambda$ and $\pi^- p \rightarrow K^0\Sigma^0$ data [53, 54, 55, 56, 57].

This policy was pursued in Ref. [19] but with the simplifications that the distortion factors, the terms within the square brackets in Eqs. (10)-(11), were not included in calculating

the resonant term of Eq. (8). Furthermore, the non-resonant $\hat{t}_{\pi N, \pi N}$ defined by Eq. (17) was only roughly estimated using the empirical πN amplitude.

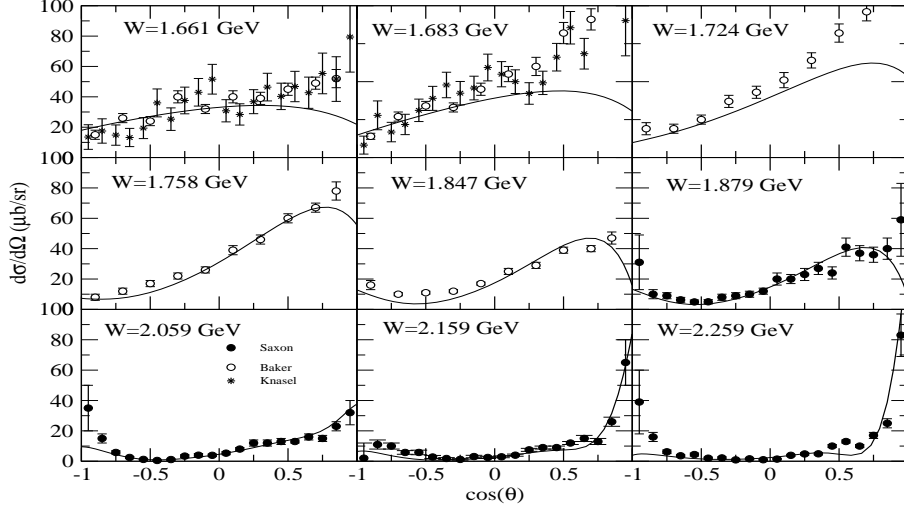


FIG. 1: Differential cross-section for the reaction $\pi^- p \rightarrow K^0 \Lambda$. The solid curves are from the fits using the coupled-channel model of this work. Data are from Refs. [53, 55].

In this work, we have corrected these two deficiencies as discussed in Section II.A and thus have refined the potentials $v_{\pi N, KY}$ and $v_{KY, KY}$ and the relevant N^* parameters.

The fitting procedure is explained in detail in Section III of Ref. [19]. Here we recall a few points to make the present Section self-consistent. In that paper, we classified the parameters in three sets (Tables I to III in Ref. [19]). Set I includes 9 couplings, the values of which are taken from the SU(3)-symmetry predictions or PDG partial decay widths; namely, $f_{\pi NN}$, $f_{\pi NN^*}$, $f_{\pi N\Lambda^*}$, and $f_{\pi N\Sigma^*}$, with $N^* \equiv S_{11}(1650)$, $D_{13}(1700)$, $P_{11}(1710)$, $P_{13}(1720)$, $\Lambda^* \equiv S_{01}(1670)$, $P_{01}(1810)$, and $\Sigma^* \equiv P_{11}(1660)$, $D_{13}(1670)$.

The adjustable parameters are in the remaining two sets. Set II includes the following coupling constants: $f_{KY N}$, $f_{KY N^*}$, $f_{KY \Delta^*}$, $f_{\pi YY}$, and $f_{\pi YY^*}$. The values extracted for those parameters within the present work are given in Table I, rows 2 to 22. Here we follow model B of Ref. [19] by allowing the parameters of the model to vary by $\pm 20\%$ around the central values taken from PDG [36] and/or from quark model [27, 28] predictions. Finally rows 23 to 31 in Table I correspond to Set III in Ref. [19].

In Figs. 1 to 4, the results of our model are compared with the differential cross-section

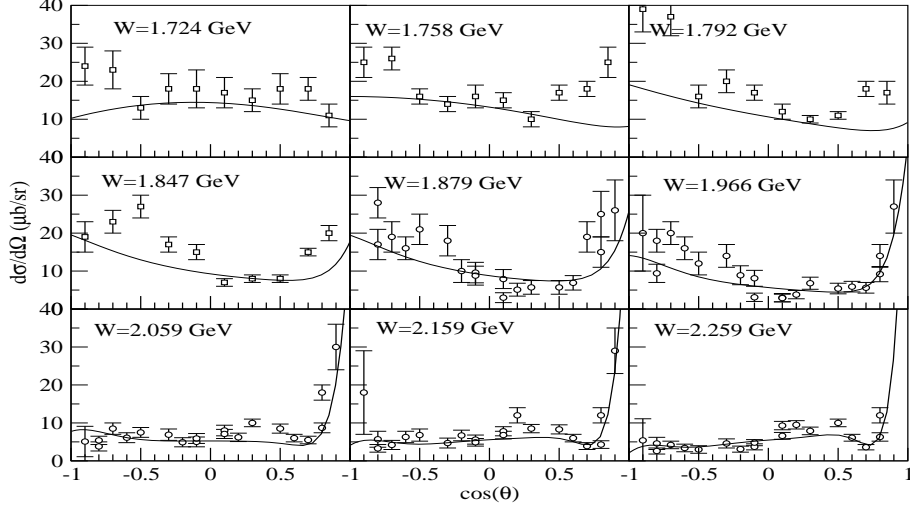


FIG. 2: Differential cross-section for the reaction $\pi^- p \rightarrow K^0 \Sigma^0$. The solid curves are from the fits using the coupled-channel model of this work. Data are from Refs. [54, 57].

and recoil hyperon polarization data [53, 54, 55, 56, 57] for processes $\pi^- p \rightarrow K^0 \Lambda$ and $\pi^- p \rightarrow K^0 \Sigma^0$.

In Figs. 1 and 2 we show the quality of our fits to the differential cross section data for $\pi^- p \rightarrow K^0 \Lambda$ and $\pi^- p \rightarrow K^0 \Sigma^0$, respectively. In Figs. 3 and 4 our results for the asymmetry data for the same reactions are depicted. The acceptable agreement between model and data, as well as $\chi^2_{d.o.f}$, compare well with our previous results [19]. Nevertheless, we consider the present model slightly more reliable than the model B in Ref. [19]. Actually, some of the coupling constants, Table I, get (much) closer to constituent quark model values [29], e.g. $f_{K\Lambda D_{13}(1700)}$, $f_{K\Sigma D_{13}(1700)}$, $f_{K\Lambda P_{11}(1710)}$, $f_{K\Lambda P_{13}(1720)}$, $f_{K\Sigma S_{31}(1900)}$, and $f_{K\Sigma P_{33}(1920)}$.

In summary, it turns out that the aforementioned improvements do not change much with respect to our previous model [19]. For the $KY \rightarrow KY$ processes, we also get comparable results to those reported in the latter paper. There is no data for $KY \rightarrow KY$ scattering to test our model. The situation might change in the near future with the advent of highly accurate data from the EPECUR [58] and J-PARC [59] projects. Those data will certainly afford deeper insights into the meson-baryon interactions. However, the results shown in Figs. 1-4 are sufficient for the purpose of studying coupled-channel effects.

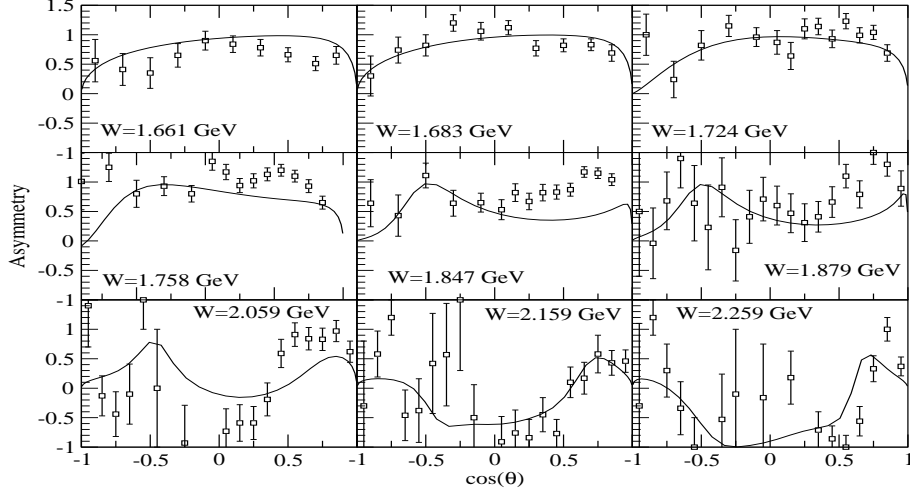


FIG. 3: Λ recoil polarization asymmetries for the reaction $\pi^- p \rightarrow K^0 \vec{\Lambda}$. The solid curves are from the fits u

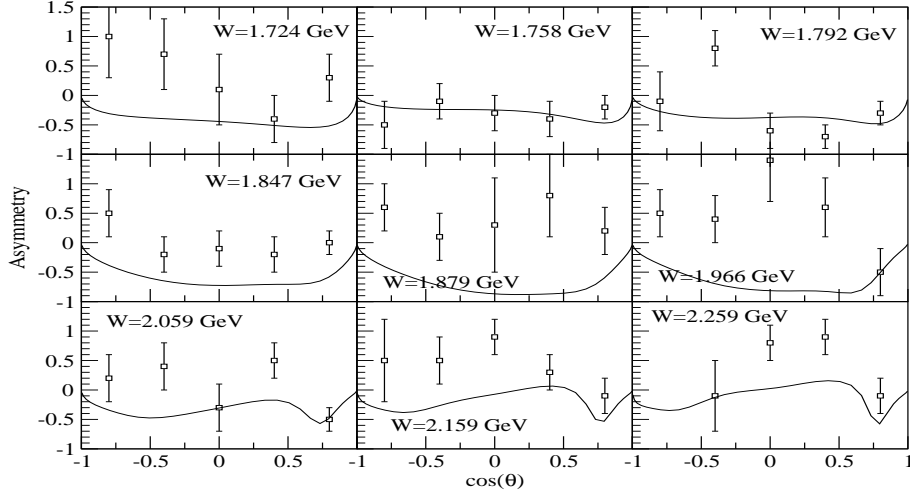


FIG. 4: Σ recoil polarization asymmetries for the reaction $\pi^- p \rightarrow K^0 \vec{\Sigma}^0$. The solid curves are from the fits using the coupled-channel model of this work. Data are from Ref. [57].

B. $\gamma p \rightarrow K^+ \Lambda$ Reaction

We have performed a thorough study of all the latest relevant data (Table II). The data released in December 2005 by LEPS [6] are not included in our fitted data base. However, they are depicted in the relevant figures below and briefly discussed.

The strong interaction channels amplitudes $v_{\pi N, KY}$ and $t_{KY, KY}$ are determined above, and $t_{\gamma N, \pi N}$ computed from Eq. (18).

Lab/Collaboration	Observable	# of data points	Ref.
ELSA/SAPHIR	Differential cross-section	720	[3]
JLab/CLAS	Differential cross-section	1068	[1]
JLab/CLAS	Recoil polarization asymmetry	233	[2]
SPring-8/LEPS	Polarized beam asymmetry	44	[5]
Bonn synchrotron	Polarized target asymmetry	3	[61]

TABLE II: Data sets investigated in the present work. Here, we have not included 268 cross-section data points from CLAS [1] for $E_\gamma > 2.6$ GeV ($W \geq 2.4$ GeV), in order to concentrate on the baryon resonances energy range.

For both non-resonant and resonant $\gamma p \rightarrow K^+ \Lambda$ amplitudes we use a constituent quark model [23, 60]. We recall that the resonant term of Eq. (7) contains a term

$$t_{\gamma N, KY}^R = v_{\gamma N, KY}^R [1 + G_{KY} t_{KY, KY}], \quad (26)$$

with

$$v_{\gamma N, KY}^R = \frac{\Gamma_{N^*, \gamma N}^\dagger \Gamma_{N^*, KY}}{E - M_{N^*} + i\Gamma^{tot}(E)/2}. \quad (27)$$

To use the N^* contributions defined by Eqs. (23)- (25), we replace the above expression by

$$v_{\gamma N, KY}^R = C_{N^*} M_{N^*}^{CQM}, \quad (28)$$

where $M_{N^*}^{CQM}$ is calculated [23] from the constituent quark model. The $SU(6) \otimes O(3)$ symmetry breaking coefficient C_{N^*} , Eq. (28), are treated as constrained adjustable parameters [22, 24] in fitting the data.

1. Model search

In this Section, we explain the procedure used to build a model for all available data.

Here we would like to emphasize that the CLAS [2] and SAPHIR [3] data released in 2004, with some 2000 data points for differential cross-sections, showed significant discrepancies

with each other. This fact led the phenomenologists either to concentrate on one of the two sets or produce one model per data set. This uncomfortable situation is now significantly cured thanks to the CLAS Collaboration's new data [1], made available in 2005. In an earlier attempt [21], we underlined this improvement in experimental data base and reported our preliminary results obtained with respect to both SAPHIR 2004 and CLAS 2005 data.

Table II summarizes the content of the data base used to determine the adjustable parameters of our approach; namely, known resonances strengths. Additional parameters due to the introduction of new resonances are discussed in Section III B 2. Differential cross-section data provide, of course, the main constraints on the model ingredients. Consequently, our starting point was to fit separately the CLAS and SAPHIR cross-section data, for which the reduced χ^2 s turned out to be 2.1 and 1.3, respectively. The significantly larger $\chi_{d.o.f}^2$ found using the CLAS data is due to their smaller uncertainties compared to those of SAPHIR data. However, this fact might not be the only source of the difference in χ^2 s. Actually, two considerations are in order here:

i) The earlier data from CLAS [2] showed significant discrepancies with SAPHIR [3] data. Although the new CLAS [1] data set has significantly reduced those discrepancies, in some phase space regions results from the two data set differ still by more than 2σ ;

ii) The strengths of resonances, which constitute our main adjustable parameters, are rather tightly constrained by $SU(6) \otimes O(3)$ symmetry. Consequently, the fact that we obtain a much better $\chi_{d.o.f}^2$ for the SAPHIR data compared to the one for the CLAS data leads to the conclusion that our approach is more in line with the SAPHIR differential cross-section data than with CLAS results.

Keeping the above considerations in mind, we present two models here:

i) Model M_1 : all SAPHIR and most recent CLAS differential cross-sections (first two rows in Table II) were fitted simultaneously.

ii) Model M_2 : all cross-section and polarization asymmetries (Table II) were fitted simultaneously.

Extracted values for the eleven adjustable parameters are given in Table III. That Table contains the KYN coupling constant and the strengths of known resonances with masses ≤ 2 GeV. The higher-mass, known resonances are treated as degenerate in a compact way [23, 51] and bear no symmetry breaking coefficients. Moreover, the Roper resonance, although explicitly present in our approach, does not contribute to the reaction mechanism due to its

low mass with respect to the reaction threshold. In addition to those known resonances, we also introduce 3 adjustable parameters per each of three newly proposed S_{11} , P_{13} , and D_{13} resonances, as discussed below (see Table IV in Section III B 2).

Parameter	Model M_1	Model M_2
$g_{KN\Lambda}$	8.02	8.00
$C_{S_{11}(1535)}$	-0.85	-0.82
$C_{S_{11}(1650)}$	-0.10	-0.22
$C_{P_{11}(1710)}$	1.79	-1.08
$C_{D_{13}(1520)}$	-2.00	-2.00
$C_{D_{13}(1700)}$	0.16	-0.19
$C_{P_{13}(1720)}$	-0.40	0.05
$C_{P_{13}(1900)}$	0.80	1.60
$C_{D_{15}(1675)}$	-0.09	0.22
$C_{F_{15}(1680)}$	1.43	1.99
$C_{F_{15}(2000)}$	1.28	1.59
$\chi_{d.o.f}^2$	2.49	3.32

TABLE III: Kaon-nucleon-hyperon coupling constant, $SU(6) \otimes O(3)$ symmetry breaking coefficient C_{N^*} as in Eq. (28), and reduced χ^2 for models M_1 and M_2 .

Here we would like to comment about the extracted values of adjustable parameters. The coupling constant $g_{KN\Lambda}$ is very close to its lowest limit [62] within broken $SU(3)$ -symmetry. This parameter, like several other adjustable ones, is driven by CLAS data. Actually fitting only the SAPHIR data leads to $g_{KN\Lambda}=9.70$. Finally, the $\chi_{d.o.f}^2$ for the model M_1 is significantly higher than obtained by fitting only the SAPHIR data. Actually the integrated χ^2 for the latter data set increases by more than a factor of 2, i.e. the adjustable parameters are driven by the CLAS data. However, in going from the model M_1 to M_2 that integrated χ^2 stays stable, while the integrated χ^2 for CLAS data increases by roughly 30%. Moreover, in the integrated χ^2 s for the models M_1 and M_2 , CLAS data represents roughly 55% and 48%, respectively, while SAPHIR data account for about 45% and 29%, respectively. These results indicate that, within our approach, the SAPHIR data show larger compatibilities with the polarization data, than does the CLAS data.

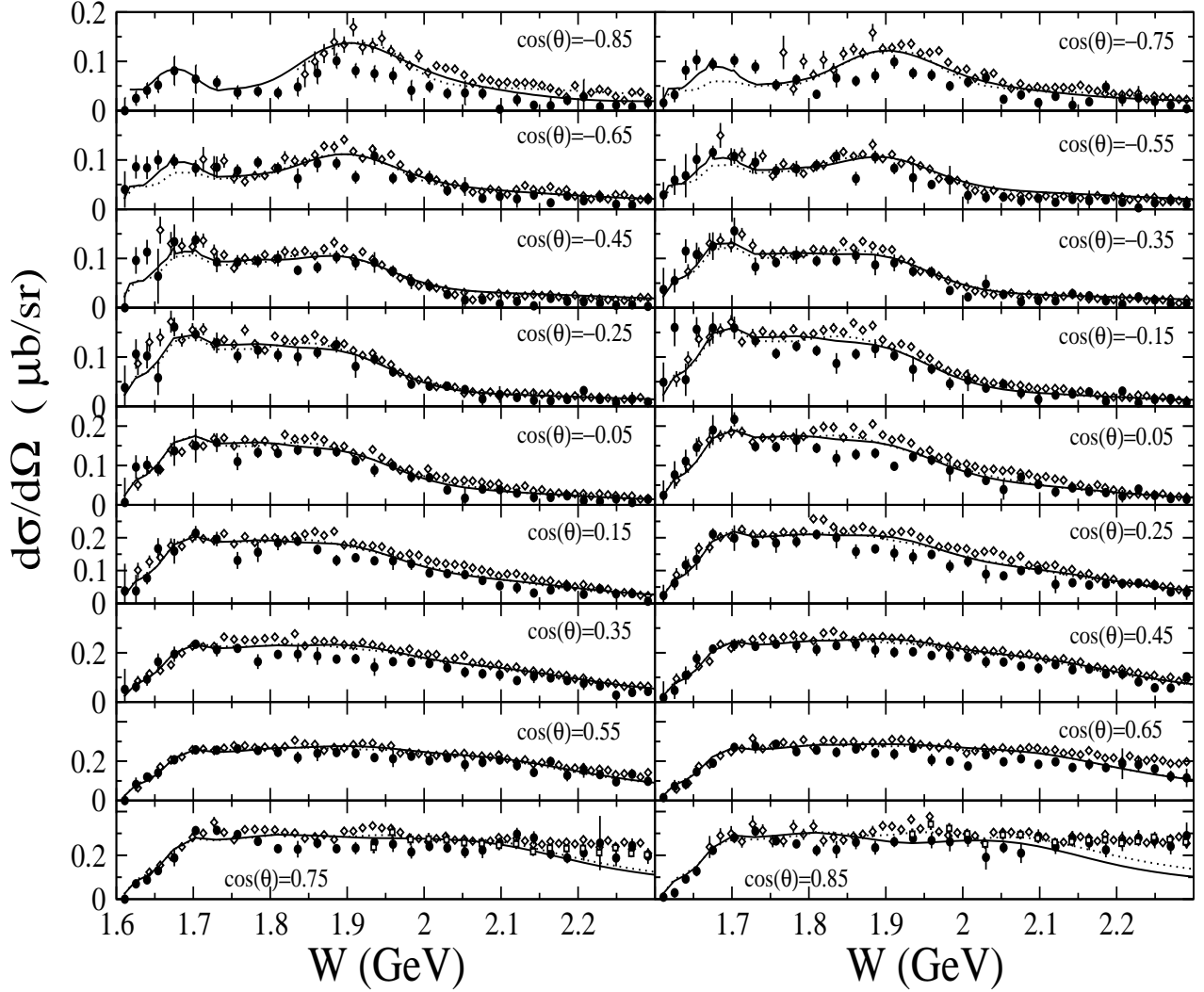


FIG. 5: Differential cross-section for the reaction $\gamma p \rightarrow K^+ \Lambda$ as a function of total center-of-mass energy. Dotted and solid curves correspond to models M_1 and M_2 respectively. Data are from Ref. [1] (open diamonds), Ref. [3] (full circles), and LEPS [6] (open squares in the cells corresponding to $\cos\theta = 0.75$ and 0.85). Plotted data from Ref. [1] are measured at $\cos(\theta)' = \cos(\theta) + 0.05$.

In Figs 5 to 8, results for models M_1 and M_2 are compared with the most recent data.

In Fig. 5 excitation functions at 19 angles, for $\theta_K \approx 25^\circ$ to 150° are shown as a function of total center-of-mass energy for $W = 1.6$ GeV to 2.3 GeV. Except in very few phase space regions, the two models give identical results. Given the discrepancies between the two fitted

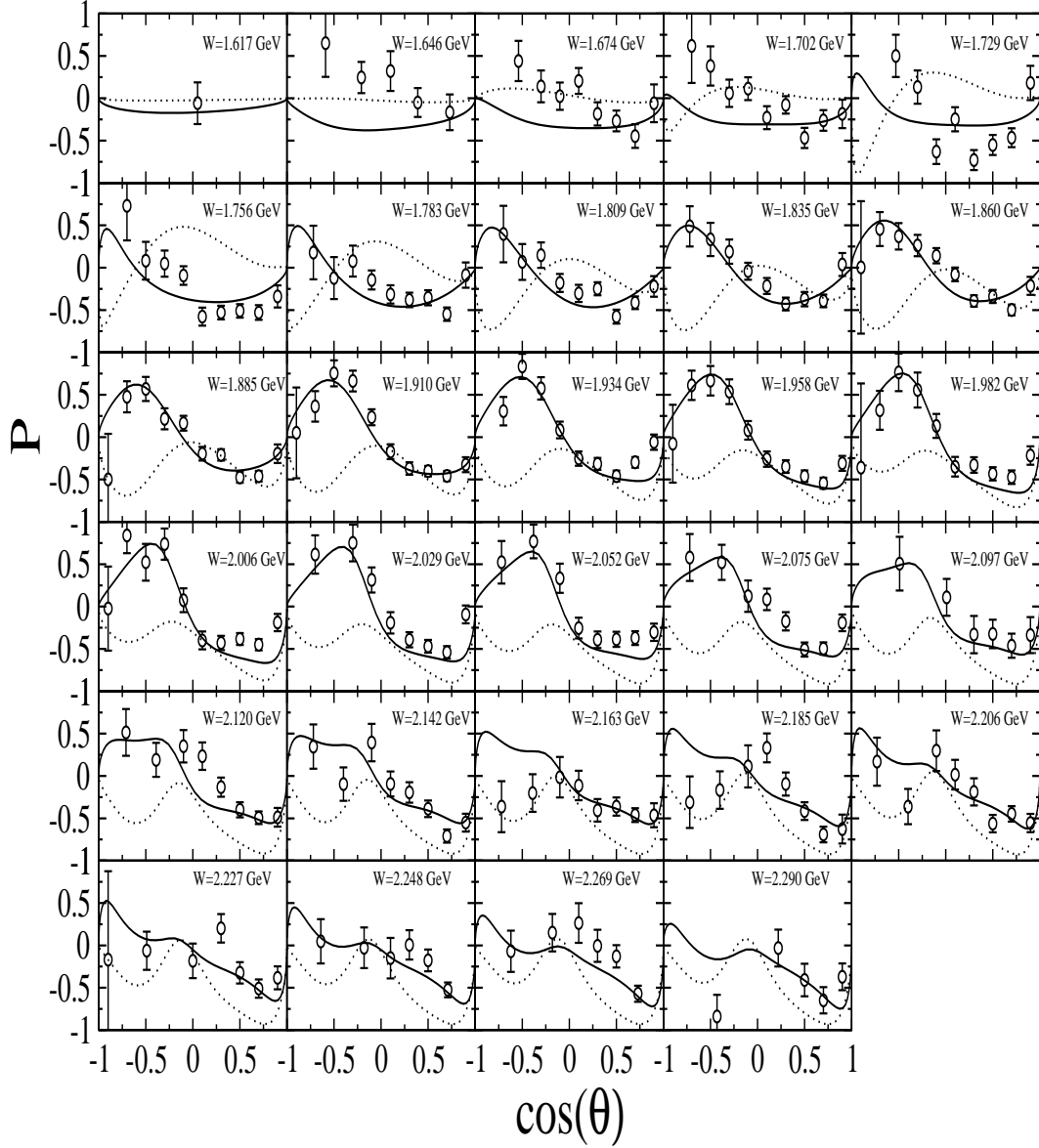


FIG. 6: Angular distribution for recoil Λ polarization asymmetry for the reaction $\gamma p \rightarrow K^+ \bar{\Lambda}$. Curves as in Fig. 5. Data are from Ref. [2].

data sets, our models give an acceptable account of the differential cross-sections. In the same figure, we show also the very recent LEPS data [6] for $\cos\theta = 0.75$ and 0.85 . They turn out to be closer to the CLAS data, rather than to SAPHIR results.

With respect to the polarization observables, we recall that model M_1 (dotted curve) has been obtained by fitting only the cross section-data. So, in Figs 6 to 8, dotted curves are

predictions. While the full curves (model M_2) result from fits to differential cross-section and polarization observables data.

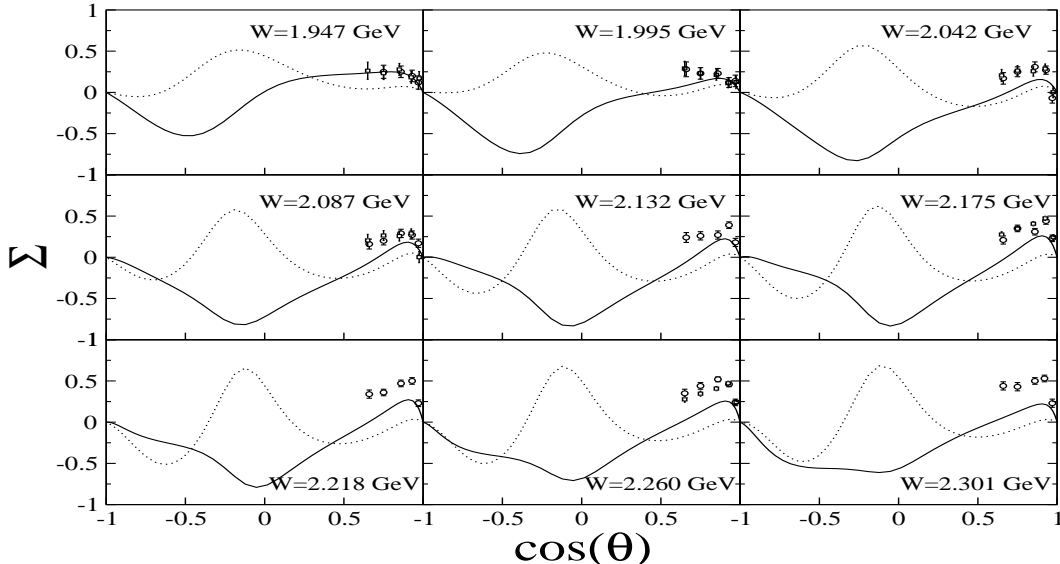


FIG. 7: Angular distribution for polarized beam asymmetry for the reaction $\vec{\gamma}p \rightarrow K^+\Lambda$. Curves as in Fig. 5. Data are from Ref. [5] (circles) and Ref. [6] (squares).

In Fig. 6 angular distribution of polarized recoil Λ asymmetry is depicted for $W \approx 1.6$ GeV to 2.3 GeV. Models M_1 and M_2 give significantly different results and the latter model reproduces the data quite well, except for a few lowest energy ones. It is worthwhile mentioning that although recoil data represents less than 10% of the data base points, and contribute to the total χ^2 by the same percentage, they have a significant effect in the determination of the model ingredients.

The polarized photon beam asymmetry, Fig. 7, data stand for less than 2% of data base points, but generate about 13% of the total χ^2 . We recall that the fitted data come from Ref. [5] and are shown as open circles in all 9 cells of Fig. 7; while the very recent data [6], depicted as open squares, were not included in the fitted data base. Here, model M_2 (solid curves) shows an improvement over M_1 (dotted curves) when compared with the data. According to our results, further measurements of this observable around $\theta_K \approx 90^\circ$ would put strong constraints on the models search.

Polarized target asymmetry has been measured only by one group [61] about 3 decades

ago. For completeness, we compare our models with those few data points, Fig. 8, showing that the model M_2 gives a better agreement with those data. Contribution of those data to the total χ^2 is around 0.1%.

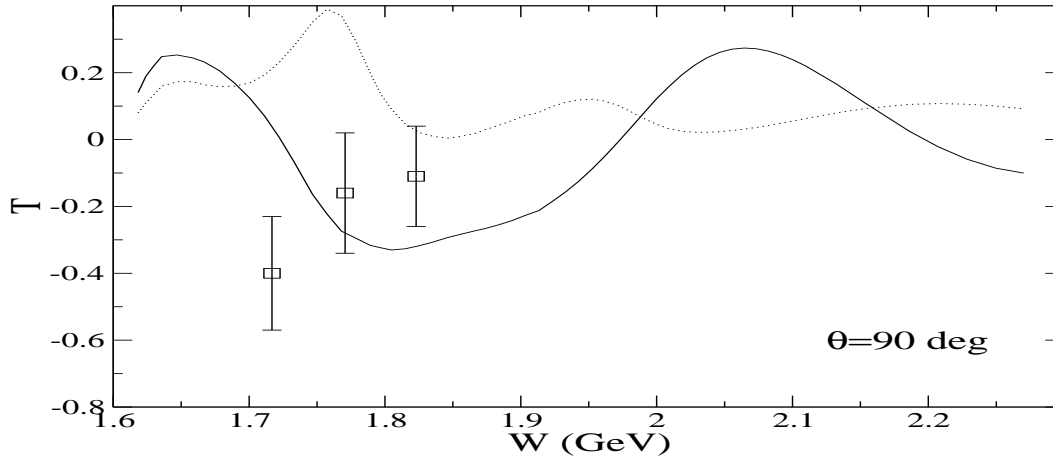


FIG. 8: Excitation function for Polarized target asymmetry for the reaction $\gamma \vec{p} \rightarrow K^+ \Lambda$. Curves as in Fig. 5. Data are from Ref. [61].

In summary, the model M_2 provides a reasonable description of the whole data base Figs. 5-8 and the comparisons of the resulting parameters listed in Table III indicate the importance of having polarization observables data in the study of N^* resonances.

2. Search for new resonances

For about three decades, several approaches have been predicting baryon resonances not seen in extensively investigated πN channels. issues related to those missing resonances have recently been reviewed [30, 31, 63].

The search for missing resonances has been initiated by predictions formulated in three pioneer approaches: i) Relativized quark formalism [26, 27, 28, 29], ii) Algebraic approach [31], iii) Hypercentral constituent quark model [32].

Moreover, several authors have reported about three missing resonances with masses between 1.8 and 2 GeV, namely, S_{11} , P_{13} , and D_{13} . In the present work, we have investigated possible contributions from such resonances to the $\gamma p \rightarrow K^+ \Lambda$ reaction mechanism. Before

presenting our results, we give a brief account of findings reported in the literature with respect to those resonances. It is worthwhile keeping in mind that all the results mentioned below and referring to the CLAS data, use the CLAS 2004 results [2] and not the more recent ones [1]. So, conclusions based on those works have to be updated.

a) Third S_{11}

The extracted values for the mass and width of a new S_{11} are close to those predicted by the authors of Ref. [39] ($M = 1.712$ GeV and $\Gamma = 184$ MeV), as a KY bound state.

The chiral constituent quark approach used in the present work served [23, 40] in the interpretation of the $\gamma p \rightarrow \eta p$ data and put forward strong indications for a third S_{11} with $M = 1.780$ GeV and $\Gamma = 280$ MeV.

For the one star $S_{11}(2090)$ resonance [36] and where the mass ranges between 1.880 GeV to 2.180 GeV, the Zagreb group's coupled channel analysis [41] produces the following values $M = 1.792 \pm 0.023$ GeV and $\Gamma = 360 \pm 49$ MeV. The same one star resonance was invoked in the 1.932 GeV to 1.959 GeV range, using a reggeized isobar model [42] to investigate the $\gamma p \rightarrow \eta' p$ reaction. Still another isobar approach [44] investigation of the $\gamma p \rightarrow \eta p$ puts forward an S_{11} resonance with $M = 1.825$ GeV and $\Gamma = 160$ MeV.

A self-consistent analysis of pion scattering and photoproduction within a coupled channel formalism, indicates [43] the existence of a third S_{11} resonance with $M = 1.803 \pm 0.007$ GeV.

Finally, one of the main recent experimental sources on baryon resonances comes from the BES Collaboration [45, 46], using J/Ψ decay channels. In an early stage, they concentrated [45] on neutral pion and η final states: $J/\Psi \rightarrow \bar{p}p\pi^0, \bar{p}p\eta$. The authors could identify the two known S_{11} resonances and extracted their masses and widths in agreement with the PDG values. They found a structure at $M = 1800$ MeV, the quantum numbers of which could not be identified because of lack of statistics.

b) Third P_{13}

Very recently, the BES Collaboration has released [46] data for charged pion final states: $J/\Psi \rightarrow \bar{p}\pi^+n, \bar{n}\pi^-p$. Besides again identifying the two known S_{11} resonances, they put forward the following interesting results: i) The Roper P_{11} resonance's mass and width are reported, $M = 1358 \pm 6 \pm 16$ MeV and $\Gamma = 179 \pm 26 \pm 50$ MeV, to be significantly smaller than their widely used values. ii) A fourth resonance was identified by the authors with $M = 2068 \pm 3_{-40}^{+15}$ MeV and $\Gamma = 165 \pm 14 \pm 40$ MeV, $3/2^+$ spin parity.

c) Third D_{13}

The first indication of a new D_{13} with a mass close to 1.9GeV was suggested by Mart and Bennhold [8], who interpreted the SAPHIR 1998 data [64] within an isobar approach. Subsequently, it was shown that those data could be reproduced both within an isobar model [65], embodying off-shell effects, and a constituent quark approach [24]. Moreover, recent data [3] released in 2004 by the SAPHIR Collaboration did not confirm the structure reported in their 1998 paper. Afterwards, Mart et al. [66] reached the conclusion that the manifestations of such a resonance appeared to be poorly-determined.

Within an isobar model, including s - and t -channel contributions in the tree approximation, Anisovich *et al.* [67] analyzed the processes $\gamma p \rightarrow \pi N, \eta N, K^+\Lambda, K^+\Sigma^0, K^0\Sigma^+$ and suggested a new D_{13} with $M = 1875 \pm 25$ and $\Gamma = 80 \pm 20$. The authors report a less strong indication for an additional D_{13} with $M = 2166^{+50}_{-80}$ and $\Gamma = 300 \pm 65$, that they attribute to the $N^*(2080)$ of PDG. However, recent results from the CB-ELSA Collaboration [68] on the $\gamma p \rightarrow N^*(\Delta^*) \rightarrow \pi^0 p$ puts this latter two star resonance at $M = 1943 \pm 17$ and $\Gamma = 82 \pm 20$.

A hybrid isobar plus Regge model has been developed by Corthals et al. [15]. According to the Regge background model used, a $D_{13}(1895)$ appears or vanishes. The authors suspect a role for significant final state interactions not included in their approach. Such effects are also absent in all isobar models discussed above.

Such effects, as well as intermediate state reactions, are of course embodied in the coupled-channel approaches based on the K-matrix formalism developed by the Giessen [16] and Groningen [17] groups, though both groups use isobar models for the direct processes. Neither of those works show evidences for new resonances. However, the Giessen group fitted separately SAPHIR and CLAS 2004 data and the Groningen group used only SAPHIR data.

Finally, an investigation [47] of the relations between the S -matrix and time delay in πN interactions, concluded that a $D_{13}(1940)$ could appear.

Given the results from other investigations outlined above, we proceed to the presentation of our findings with respect to those new resonances.

In Section III B 1, we presented our model and made comparisons with all available data sets. In this Section, we use the model M_2 discussed in Section III B 1, in order to investigate possible manifestations of three missing resonances: S_{11} , P_{13} , and D_{13} . For that purpose, we have attributed 3 adjustable parameters (mass, width, and strength) to each of those resonances in the minimization procedure. The extracted parameters are given in Table IV.

New resonance	Property	Model M_1	Model M_2
S_{11}	Mass	1.833	1.806
	Width	0.288	0.300
	Strength	0.40	0.15
P_{13}	Mass	1.974	1.893
	Width	0.108	0.204
	Strength	0.12	0.28
D_{13}	Mass	1.912	1.954
	Width	0.316	0.249
	Strength	1.50	0.98

TABLE IV: Determined parameters for the third S_{11} , P_{13} , and D_{13} resonances.

In order to ascertain the role played by each additional resonance given in Table IV, we proceed as follows. In Figs. 9 to 12 we show the same observables as in Figs. 5 to 8, respectively. For each observable, the model M_2 is depicted again. The three other curves in Figs. 9 to 12 correspond to the model M_2 with one of the additional resonances switched off, without further minimizations. In those figures, the curves are: M_2 without the third S_{11} (dotted curve), P_{13} (dot-dashed curve), and D_{13} (dashed curve).

From the differential cross-sections (Fig. 9) we infer that the 3^{rd} S_{11} has a significant role in the backward hemisphere and the effect gets enhanced in going to most backward angles. The manifestations of this resonance vanish for $W \leq 1.9$ GeV. Moreover, the interference terms due to this resonance appear to be destructive in the full model M_2 .

Contributions from the 3^{rd} P_{13} resonance are confined roughly to the energy range $1.8 \leq W \leq 2.0$ GeV with increasing magnitude in going from forward to backward angles. Those contributions are rather small, but non vanishing in the whole phase space.

The most significant effects due to the 3^{rd} D_{13} resonance are around $\theta_K \approx 90^\circ$ and $W \approx 1.9$ GeV. The interference terms come out to be constructive in the forward hemisphere in the whole energy range and in the backward hemisphere for roughly $W \leq 2.0$ GeV.

The recoil hyperon polarization asymmetry, Fig. 10, shows no significant sensitivity to the third S_{11} and P_{13} except in very limited phase space regions, while switching off the 3^{rd}

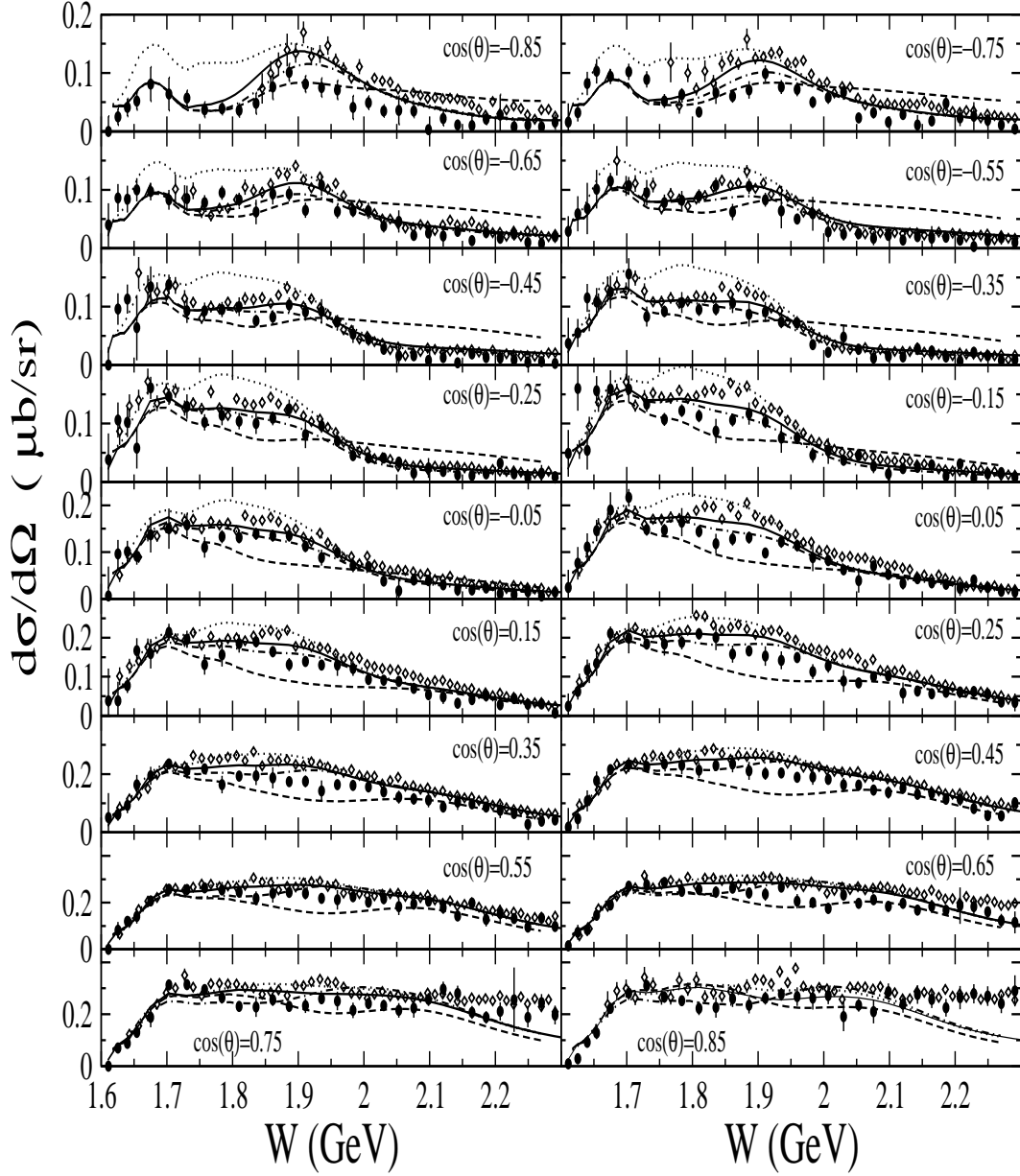


FIG. 9: Differential cross-section for the reaction $\gamma p \rightarrow K^+ \Lambda$ as a function of total-center-of-mass energy. Solid curve corresponds to the full model M_2 . Dotted, dot-dashed, and dashed curves correspond to the full model without the $3^{rd} S_{11}$, $3^{rd} P_{13}$, and $3^{rd} D_{13}$, respectively. Data are as in Fig. 5

D_{13} leads to important variations in the model values for roughly $W \geq 1.9$ GeV, mainly in the forward hemisphere.

The same trends are observed for the polarized beam asymmetry with respect to the third

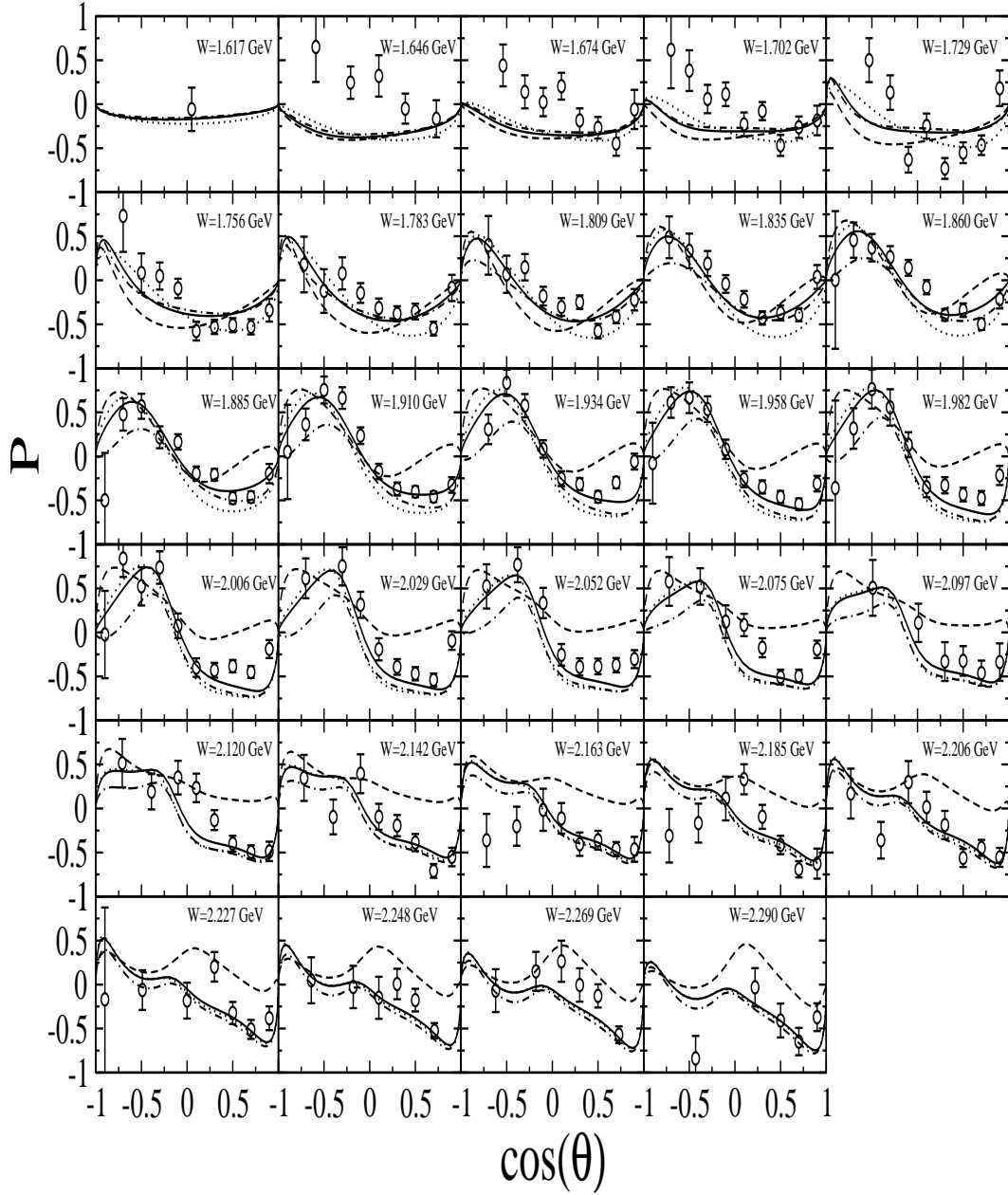


FIG. 10: Angular distribution for recoil Λ polarization asymmetry for the reaction $\gamma p \rightarrow K^+ \bar{\Lambda}$. Curves as in fig. 9. Data are from Ref. [2].

S_{11} , Fig. 11. The highest sensitivities to the two other resonances appear in the backward hemisphere and are significant for the 3^{rd} D_{13} .

For the sake of completeness, in Fig. 12 we show the excitation function at $\theta_K = 90^\circ$ for the polarized beam asymmetry. As already mentioned, this observable is by far the least

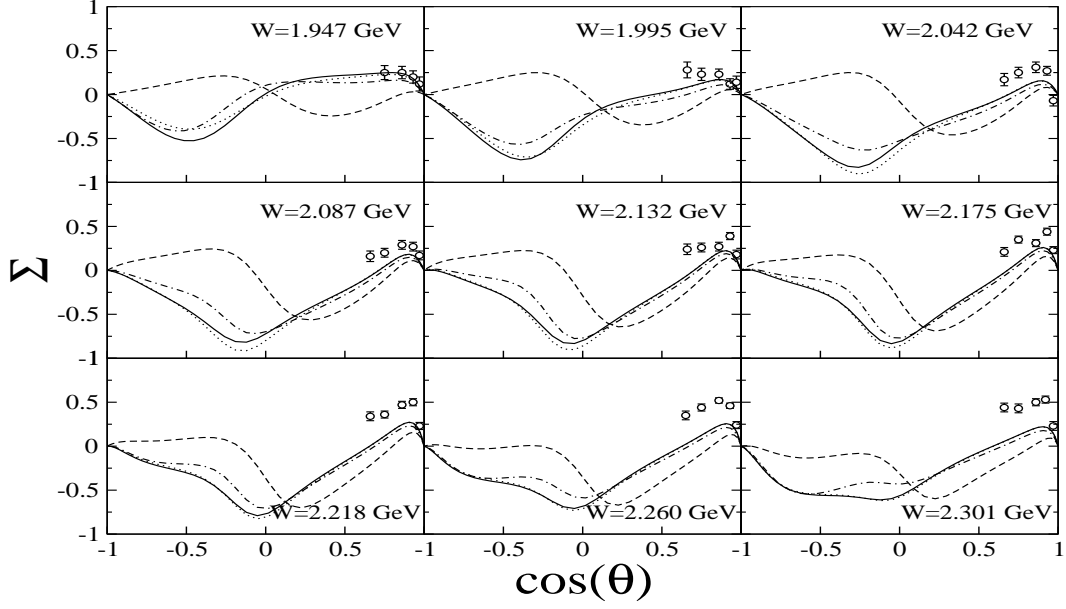


FIG. 11: Angular distribution for polarized beam asymmetry for the reaction $\vec{\gamma}p \rightarrow K^+\Lambda$. Curves as in fig. 9. Data are from Ref. [5].

studied experimentally. Our results might nevertheless indicate that the 3rd D_{13} produces a significant structure at higher energies.

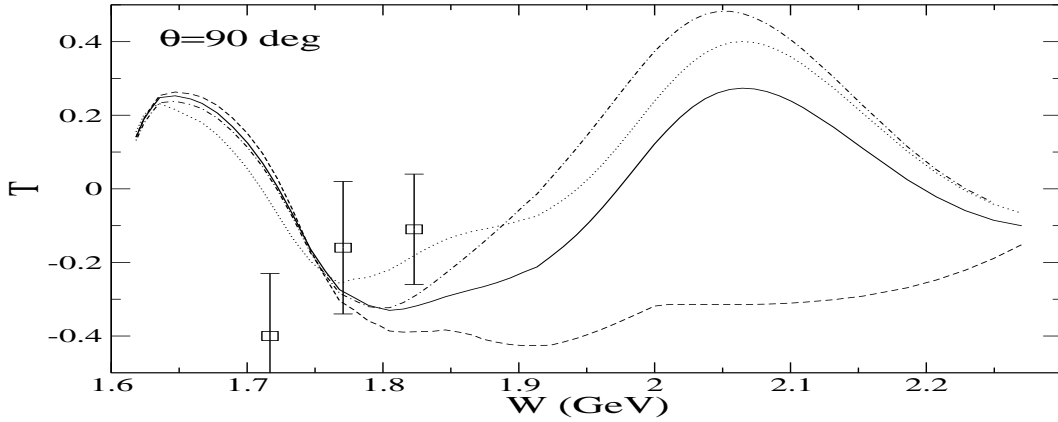


FIG. 12: Excitation function for polarized target asymmetry for the reaction $\gamma\vec{p} \rightarrow K^+\Lambda$. Curves as in fig. 9. Data are from Ref. [61].

3. Role of resonances in total and differential cross-section, and polarization observables

Total cross-sections have been extracted by both CLAS and SAPHIR collaborations. Those data were not included in our fitted data base. The prediction of our model M_2 is depicted in Fig. 13 in bold full curves. In each of the four cells, we show in addition the results of that model M_2 with only one resonance switched off at a time.

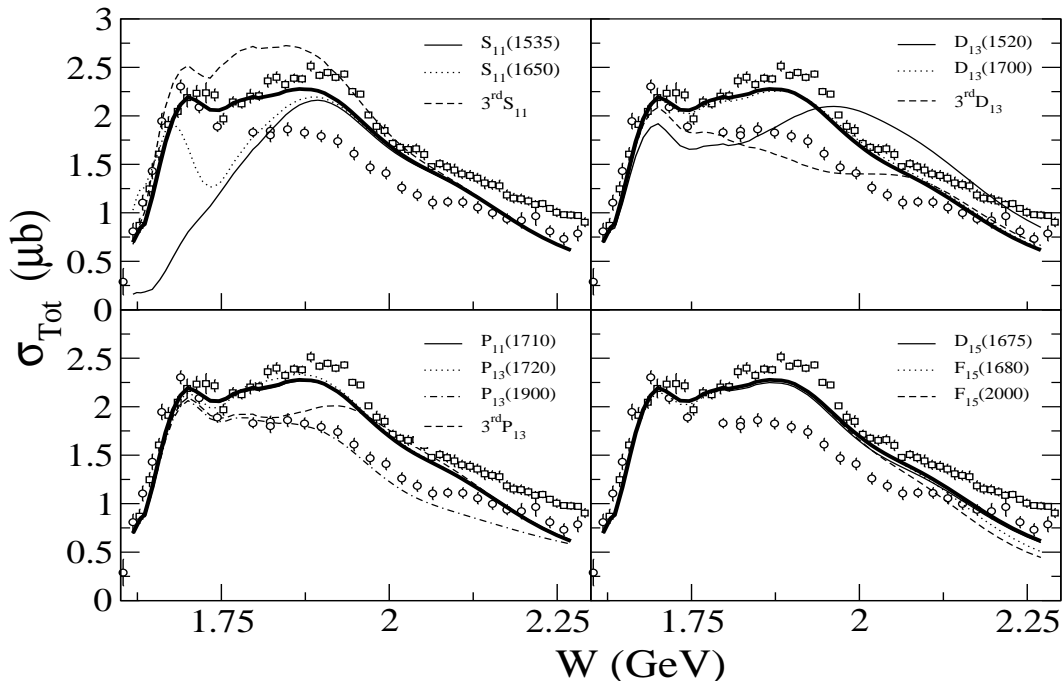


FIG. 13: Total cross-section for $\gamma p \rightarrow K^+ \Lambda$ as a function of total center-of-mass energy. The bold full curves come from the model M_2 . In each cell different curves correspond to the model M_2 with one resonance switched off, as singled out in each cell. Data are from Refs. [1, 3].

The first observation concerns the discrepancies between the two data sets. As already pointed out [21], here the discrepancies are more significant than in the case of differential cross-sections. This increased discrepancy is likely due to two facts: i) the two collaborations have performed measurements in non completely overlapping phase space regions, ii) different extrapolation methods to the unmeasured angular areas are used. The total cross-section extracted from differential cross-sections might then be misleading if included in the data base and/or used to draw strong conclusions about the reaction mechanism. There is

however a puzzling point, namely, total cross-sections for the $\gamma p \rightarrow K^+\Sigma^0$ extracted by the same collaborations, agree quite well with each other (e.g. see Figs. 20 and 21 in Ref. [1]).

The model M_2 ingredients are dominated by both data sets up to $W \approx 1.7$ GeV, by CLAS data up to $W \approx 2.0$ GeV, and by SAPHIR data above that region. Two structures appear at about 1.7 GeV and 1.9 GeV.

To gain better insight into the role played by each resonance with mass $M \leq 2$ GeV, we show curves obtained using the model M_2 by switching off each resonance. Table V gives the χ^2 for each case, without further minimizations.

In the following, we concentrate on the model M_2 in order to investigate contributions from various resonances. The points discussed below do not depend on the total cross-section data, but they embody effects from all other fitted observables. Moreover, we present the effects of each resonance with respect to the fitted data base. Here, in order to limit the number of figures, we summarize our findings in Table V, the content of which is explained below.

The integrated χ^2 in model M_2 can be written as a sum of five partial χ_i^2 s,

$$\chi^2 = \sum_{i=1}^5 \chi_i^2, \quad (29)$$

where i refers to the data sets, namely,

- $i = 1$: CLAS differential cross-sections, $(d\sigma)_{CLAS}$;
- $i = 2$: SAPHIR differential cross-sections, $(d\sigma)_{SAPHIR}$;
- $i = 3$: CLAS recoil polarization asymmetry, P ;
- $i = 4$: LEPS polarized beam asymmetry, Σ ;
- $i = 5$: Bonn polarized target asymmetry, T .

Then, for each switched off resonance, and without further minimizations, we obtain the relevant integrated $[\chi^2]_{M_2-N^*}$ and partial $[\chi_i^2]_{M_2-N^*}$ for the observable i . (Here, the subscript $M_2 - N^*$ denotes that the particular resonance N^* has been turned off.) Finally, we define the following ratio:

$$\mathcal{R}_i = \frac{[\chi_i^2]_{M_2-N^*}}{[\chi_i^2]_{M_2}}, \quad (30)$$

which gives a measure of the role of the relevant N^* with respect to the observable numbered i . In columns 3 to 7 of Table V following found intervals are reported:

$$1.0 < \mathcal{R}_i < 1.5 : *$$

$1.5 \leq \mathcal{R}_i < 1.8$: **
 $2.0 < \mathcal{R}_i < 4.4$: ***
 $6.0 < \mathcal{R}_i < 8.0$: ****
 $10.0 < \mathcal{R}_i < 13.4$: *****

Thus more stars indicate a larger role for a particular resonance on a particular observable i .

Switched off N^* ($\chi_{M_2-N^*}^2$) _{d.o.f.}	$\mathcal{R}_{(d\sigma)_{CLAS}}$	$\mathcal{R}_{(d\sigma)_{SAPHIR}}$	\mathcal{R}_P	\mathcal{R}_Σ	\mathcal{R}_T	
$S_{11}(1535)$	10.3	***	***	-	*	*
$S_{11}(1650)$	5.7	***	*	*	-	*
$S_{11}(1806)$	6.5	***	***	**	*	-
$P_{11}(1710)$	3.3	*	*	*	-	*
$P_{13}(1720)$	3.4	-	*	*	*	-
$P_{13}(1900)$	13.0	****	-	***	***	-
$P_{13}(1893)$	4.6	**	-	*	*	-
$D_{13}(1520)$	20.0	*****	***	***	-	**
$D_{13}(1700)$	3.5	*	*	*	-	*
$D_{13}(1954)$	26.4	*****	***	***	***	*
$D_{15}(1675)$	3.6	*	*	-	*	*
$F_{15}(1680)$	5.0	**	*	**	*	-
$F_{15}(2000)$	7.1	***	*	*	***	*

TABLE V: Schematic presentation of the role played by each resonance in the process $\gamma p \rightarrow K^+ \Lambda$. First column: switched off resonance in model M_2 ; second column: reduced χ^2 without further minimizations to be compared with the $(\chi_{M_2}^2)_{d.o.f.} = 3.3$ for the model M_2 (see Table III). The third to seventh columns give the intervals of \mathcal{R}_i (Eq. 30) with the number of stars as defined in the text. The three new resonances investigated here are given in bold.

In few cases, the \mathcal{R}_i is slightly smaller than 1.01, shown by a hyphen (-) in that Table.

The cell on left-top (Fig. 13) shows the effects of S_{11} resonances. The lightest resonance affects the total cross section significantly above its mass, due to constructive interference terms, and contributes clearly to the first maximum. This is also the case for the $S_{11}(1650)$, with smaller effects close to threshold. The 3rd S_{11} intervenes around 1.8 GeV and brings in

destructive interference. The first and third S_{11} resonances play important roles (Table V) in the differential cross-section data from CLAS and SAPHIR, while the second one is present only in the CLAS data.

For the P-waves (Fig. 13, left-bottom cell), $P_{11}(1710)$ and $P_{13}(1720)$ have negligible contributions and they do not appear in any of the observables (Table V). According to the same Figure and Table, the $P_{13}(1900)$ has strong manifestations within the CLAS differential cross-sections and, to a less extent, in the P and T polarization observables.

In the spin 3/2 D-waves case (Fig. 13, right-top cell), the first such state plays an important role with interference effects turning from constructive to destructive around 1.9 GeV. Table V shows that the $D_{13}(1520)$ is a crucial ingredient in reproducing the CLAS data and is important with respect to the SAPHIR results. The role of the $D_{13}(1700)$ is negligible, while the 3rd D_{13} has a clear role between roughly 1.8 GeV and 2.0 GeV (Fig. 13) and turns out to be a key element, Table V, for all observables, except T .

The spin 5/2 D- and F-waves show no significant effects in the total cross-section (Fig. 13, right-bottom cell). However, Table V underlines the importance of the F_{15} resonances, especially the second one.

To summarize this Subsection, we find that:

- Among the known resonances, the most relevant ones are: $S_{11}(1535)$, $P_{13}(1900)$, and $D_{13}(1520)$;
- Three other ones are required by data other than those from SAPHIR: $S_{11}(1650)$, $F_{15}(1680)$, and $F_{15}(2000)$;
- Among the three new resonances, the $D_{13}(1954)$ plays a crucial role in all observables, except perhaps in the beam polarization asymmetry. The $S_{11}(1806)$ plays an important role with respect to both differential cross-section data sets, and the polarized recoil data. The $P_{13}(1893)$ has a less strong role than the two previous resonances and shows up mainly in the CLAS cross-section data.

As mentioned above, all the curves with one resonance removed and depicted in Fig. 13 are obtained without further minimizations. For the sake of completeness, we shortly report about all possible configurations, after minimization, without new resonances, with one or two of them included.

The reduced χ^2 s are given in Table VI. The second column shows the result with only known resonances, with $\chi_{d.o.f}^2=5.7$. Adding either a third S_{11} or P_{13} decreases the $\chi_{d.o.f}^2$ by roughly 18% (3rd and 4th columns). While a third D_{13} improves the $\chi_{d.o.f}^2$ by about 32%. Columns 6 to 8 show the effects of combinations of two new resonances. The smallest $\chi_{d.o.f}^2$ is obtained by the S_{11} and D_{13} pairs. The last columns recalls the result for model M_2 . It is interesting to mention that the mass of those resonances stay stable within 50 MeV through the 7 configurations. These results support our conclusions above on the a) important role played by the third D_{13} , b) improvement due to an additional S_{11} , c) less significant contribution from P_{13} .

New resonances \rightarrow	None	\mathcal{S}	\mathcal{P}	\mathcal{D}	\mathcal{SP}	\mathcal{PD}	\mathcal{SD}	\mathcal{SPD}
$\chi_{d.o.f}^2$	5.7	4.8	4.7	3.9	4.2	3.6	3.4	3.3

TABLE VI: Dependence of the $\chi_{d.o.f}^2$ on all possible combinations with respect to the three new resonances.

Finally, we outline here the results obtained by using only the direct-channel calculation (with all multi-step processes turned-off). Embodying only the known resonances leads to $\chi_{d.o.f}^2 \approx 12$, to be compared to 5.7 in Table VI. The $\chi_{d.o.f}^2$ gets improved by adding new resonances and goes down to ≈ 4 when the 3 new resonances are included. Although the $\chi_{d.o.f}^2$ gets an acceptable value, some of the adjustable parameters turn out to be unrealistic.

4. Coupled-channel effects

It is important to illustrate here the differences between the coupled-channel approach presented here and the often used approximations in the literature: i) the tree-diagram models (direct-channel) neglecting multi-step phenomena, ii) the coupled-channel K-matrix approaches neglecting off-shell effects.

A tree-diagram model can be obtained from the formulation presented in section II by turning off all multi-step processes. Namely, the tree-diagram amplitude is simply

$$T_{\gamma N, KY}^{tree} = v_{\gamma N, KY} + v_{\gamma N, KY}^R, \quad (31)$$

where $v_{\gamma N, KY}$ is the non-resonant amplitude and $v_{\gamma N, KY}^R$ is the resonant amplitude calculated from Eq. (28).

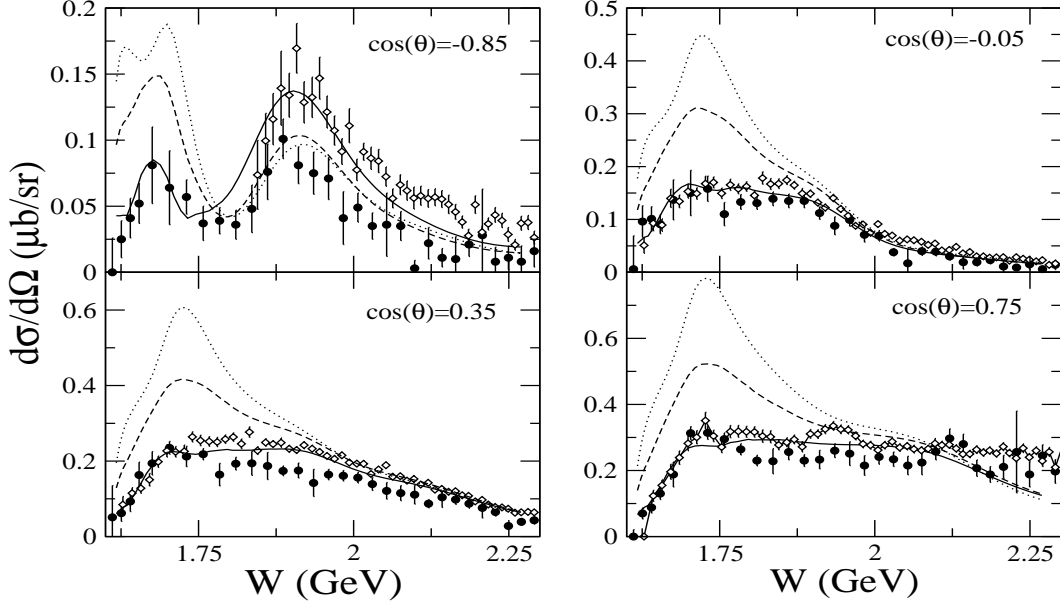


FIG. 14: Differential cross-section excitation functions at four angles for $\gamma p \rightarrow K^+ \Lambda$. The curves are: model M_2 (full curves), direct-channel results obtained by turning-off multi-step processes in the full calculation (dotted curves), and off-shell effects switched-off in the full calculation (dashed curves). Data as in Fig. 5.

The importance of the coupled-channel effects can be seen by comparing the results from Eq. (31) and the coupled-channel equations Eqs. (7)-(17). We see in Fig. 14 that when the coupled-channel effects are turned off, the resulting differential cross sections (dotted curve) would largely overestimate the cross sections; especially in the energy region $W \sim 1.6 - 2$ GeV. Obviously, the resonance parameters extracted from using the tree-diagram model will contain such theoretical uncertainties.

Moreover, within the coupled-channel formalism, the role played by off-shell effects is depicted in Fig. 14. The dashed curves there show our results when the off-shell treatment is turned off. Sizeable effects are present in the same energy range as above.

5. Meson cloud effects on N^* excitations

In the dynamical study of the Δ resonance, it was found [35, 38] that the dressed $\gamma N \rightarrow \Delta$ transition contains a large contribution due to the mechanism that the *bare* Δ state is not

directly excited by the incident photon, but by the pion first produced by the non-resonant mechanism. This contribution, commonly termed as the “meson cloud effect”, can also be identified within the coupled channel model considered here. Within the formulation presented in Section II, the meson cloud effect is contained in the terms within the square brackets of Eq. (9). Obviously such a meson cloud effect is absent in the tree-diagram model defined by Eq. (31). We also note that the calculation of these meson cloud terms involve integrations over the off-shell matrix elements of non-resonant amplitudes $t_{\gamma N, KY}$ and $t_{\gamma N, \pi N}$. Such off-shell dynamics is neglected in the K-matrix coupled-channel model [16].

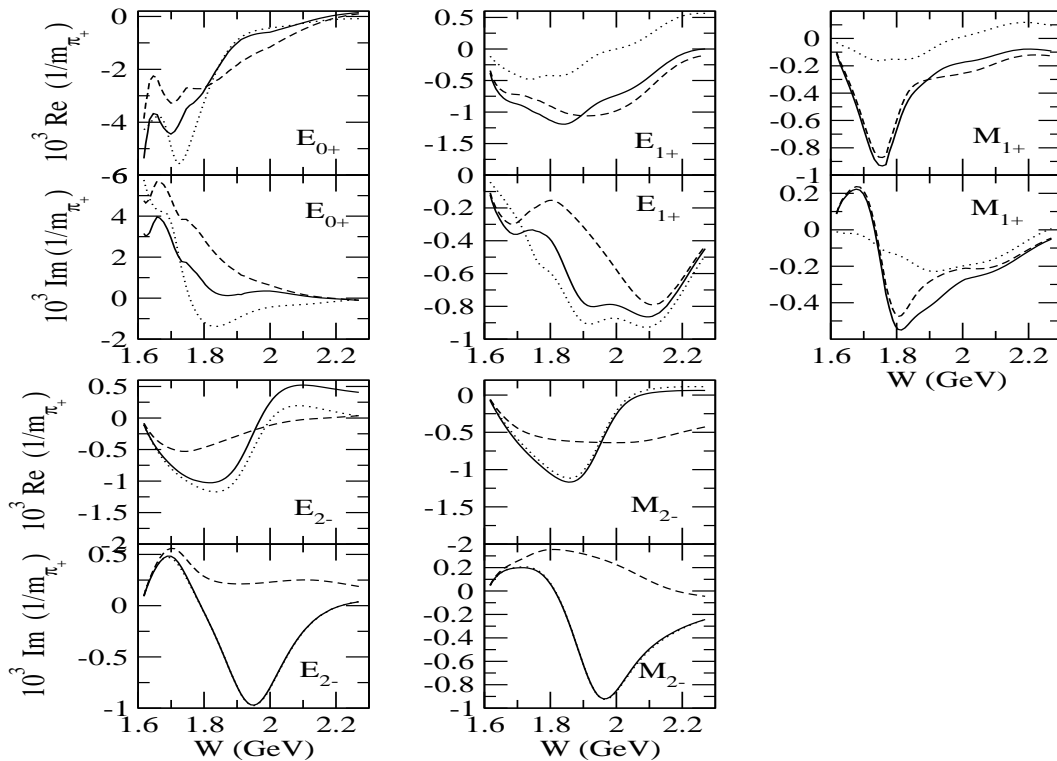


FIG. 15: The multipole amplitudes calculated from the $\gamma N \rightarrow N^* \rightarrow KY$ resonant transition for each of the three considered S_{11}^- , P_{13}^- , and D_{13}^- -wave resonances. The curves are: model M_2 (full) and the meson cloud effect Eq. (9) turned off (dotted). The dashed curves correspond to the relevant third resonances switched off: $S_{11}(1806)$ in E_0^+ , $P_{13}(1893)$ in E_1^+ and M_1^+ , and $D_{13}(1954)$ in E_2^- and M_2^- .

The meson cloud effect on the resonances can be illustrated by comparing the multipole amplitudes calculated with and without the terms within the square brackets of Eq. (9).

Other quantities of the coupled-channel equations are kept the same in these two calculations. In Fig. 15, the full curves correspond to the full M_2 model, while the dotted lines are obtained by turning off terms within the square brackets of Eq. (9), showing the importance of meson cloud effects in interpreting the extracted N^* parameters. To further understand the meson cloud effects, we need to extend the present model to investigate electroproduction data such that the Q^2 evolution of the multipole amplitude can be extracted, as has been done in the study of the Δ resonance of Ref. [35, 38]. Our effort in this direction will be reported elsewhere.

In that Figure the dashed lines are obtained by switching off the relevant third resonances investigated here. These results confirm our conclusions in Sec.III B 3, namely, the $D_{13}(1954)$ plays a crucial role, $S_{11}(1806)$ has a significant effect, and contributions from the $P_{13}(1893)$ resonance are smaller than those from the two other new resonances.

IV. SUMMARY AND CONCLUSIONS

The main motivation of the present work is the interpretation of recent associated strangeness photoproduction on the proton, which require coupled-channel formalisms. In the present work we have focused on the intermediate state πN , as well as the intermediate and final states KY interactions.

We have first applied our formalism to the $\pi p \rightarrow KY$ and $KY \rightarrow KY$ ($K \equiv K^0, K^+$, and $Y \equiv \Lambda, \Sigma^0, \Sigma^+$) by improving our previous work [19] and comparing successfully our results with the existing data. We have hence fixed the interactions $v_{\pi N, KY}$ and $v_{KY, KY}$, as well as relevant N^* parameters. Then, starting from the formalism reported in Ref. [18], we have developed a more advanced coupled-channel approach. For the direct $\gamma p \rightarrow K^+\Lambda$ we have used a chiral constituent quark model [23]. The relevant data have been used to fix the strengths of intervening resonances within the broken $SU(6) \otimes O(3)$ symmetry.

Good fits to all of the available data of $\pi^- p \rightarrow K^0 \Sigma^0$, $\pi^- p \rightarrow K^0 \Sigma^0$, and $\gamma p \rightarrow K^+\Lambda$ have been achieved. We have demonstrated that the coupled-channel effect can strongly change the results from the often used tree-diagram models. We have also found that the meson cloud effects on $\gamma N \rightarrow N^*$ are important in interpreting the extracted resonance parameters.

This work shows that the most relevant known resonances in $\gamma p \rightarrow K^+\Lambda$ process are: $S_{11}(1535)$, $P_{13}(1900)$, $D_{13}(1520)$, and to a lesser extent $F_{15}(1680)$ and $F_{15}(2000)$. Contribu-

tions from three new nucleon resonances have been extensively studied leading to convincing manifestations of a D_{13} resonance with $M = 1.954$ GeV and $\Gamma = 249$ MeV. Rather significant effects due to a S_{11} resonance with $M = 1.806$ GeV and $\Gamma = 300$ MeV is observed. A non negligible role is also found for a P_{13} resonance with $M = 1.893$ GeV and $\Gamma = 204$ MeV. Accounts of indications on those resonances from other sources were summarized.

As a next step, the very new data from LEPS [6] and forthcoming polarized beam data from GRAAL and beam-recoil double polarization asymmetries from CLAS [69] and GRAAL, will hopefully clear up the experimental situation with respect to some inconsistencies within the present data base. Moreover, the ongoing extension of our approach to the $\gamma p \rightarrow K^+\Sigma^0, K^0\Sigma^+$ channels will certainly bring in deeper insights to the associated strangeness photoproduction processes.

Finally, we emphasize that the present coupled-channel calculation is still far from being complete. While the coupling with the πN channel has been included, it is necessary to extend the present investigation to include the other channels, in particular the two-pion channels. Thus the extracted resonance parameters should be considered preliminary. But they could serve as the starting points for performing a more advanced coupled-channel calculation including additional meson-baryon channels (e.g. $\eta N, \omega N, \pi\pi N$ ($\sigma N, \pi\Delta, \rho N$)) and to fit simultaneously all meson photoproduction data.

Acknowledgments

We are grateful to Wen-Tai Chiang, Zhenping Li, and Tao Ye for their contributions to earlier stages of this work. We thank Reinhard A. Schumacher and Mizuki Sumihama for having communicated to us the CLAS and LEPS data; respectively. The gracious hospitality during stays in Pittsburgh and visits to Argonne are very much appreciated by BJD. This work is supported by the U.S. Department of Energy, Office of Nuclear Physics Division, under contract N^o W-31-109-ENG-38, and by the US National Science Foundation under grant PHY-0244526.

APPENDIX A: DERIVATION OF SCATTERING EQUATIONS

In this appendix, we show that the scattering Eqs. (1)-(6) in Section II A can be derived exactly by using the formal scattering theory given in, for example, the text book of Goldberger and Watson [48]. We start with the following Hamiltonian

$$H = H_0 + v + w, \quad (\text{A1})$$

where H_0 is the free Hamiltonian, v is the non-resonant meson-baryon (MB) interaction with $MB = \gamma N, KY, \pi N$, and

$$w = \Gamma^\dagger \frac{1}{E - H_0} \Gamma, \quad (\text{A2})$$

defines the resonant excitation by the $N^* \rightarrow MB$ vertex interaction Γ .

The MB reaction amplitude $T(E)$ is then defined [48] by (we omit $+i\epsilon$ in the propagator $1/[E - H_0 + i\epsilon]$)

$$T(E) = (v + w)[1 + \frac{1}{E - H_0} T(E)], \quad (\text{A3})$$

or

$$T(E) = (v + w)[1 + \frac{1}{E - H_0 - v - w} (v + w)] \quad (\text{A4})$$

$$= (v + w) \frac{1}{E - H_0 - v - w} (E - H_0). \quad (\text{A5})$$

Comparing Eqs. (A3) and (A5), we thus have

$$[1 + \frac{1}{E - H_0} T(E)] = \frac{1}{E - H_0 - v - w} (E - H_0). \quad (\text{A6})$$

We further define the non-resonant scattering matrix t by

$$t(E) = v[1 + \frac{1}{E - H_0} t(E)] \quad (\text{A7})$$

$$= v[1 + \frac{1}{E - H_0 - v} v] \quad (\text{A8})$$

$$= [1 - v \frac{1}{E - H_0}]^{-1} v \quad (\text{A9})$$

$$= [1 + t(E) \frac{1}{E - H_0}] v. \quad (\text{A10})$$

Eqs. (A7) and (A8) lead to

$$[1 + \frac{1}{E - H_0} t(E)] = \frac{1}{E - H_0 - v} [E - H_0], \quad (\text{A11})$$

and Eqs. (A9) and (A10) to

$$\left[1 - v \frac{1}{E - H_0}\right]^{-1} = 1 + t(E) \frac{1}{E - H_0}. \quad (\text{A12})$$

Using Eqs. (A6), (A9), and (A12), Eq.(A3) can be written as

$$\begin{aligned} T(E) &= \left[1 - v \frac{1}{E - H_0}\right]^{-1} v + \left[1 - v \frac{1}{E - H_0}\right]^{-1} w \left[1 + \frac{1}{E - H_0} T(E)\right] \\ &= t(E) + \left[1 + t(E) \frac{1}{E - H_0}\right] w \left[1 + \frac{1}{E - H_0} T(E)\right] \\ &= t(E) + \left[1 + t(E) \frac{1}{E - H_0}\right] w \frac{1}{E - H_0 - (v + w)} (E - H_0). \end{aligned} \quad (\text{A13})$$

We next use the property that

$$\frac{1}{E - H_0 - (v + w)} = \left[1 + \frac{1}{E - H_0 - v} t_w\right] \frac{1}{E - H_0 - v}, \quad (\text{A14})$$

with

$$t_w = w + w \frac{1}{E - H_0 - v} t_w, \quad (\text{A15})$$

to write Eq.(A13) as

$$\begin{aligned} T(E) &= t + \left[1 + t(E) \frac{1}{E - H_0}\right] \left[w + w \frac{1}{E - H_0 - v} t_w\right] \frac{1}{E - H_0 - v} [E - H_0] \\ &= t + \left[1 + t(E) \frac{1}{E - H_0}\right] t_w \frac{1}{E - H_0 - v} [E - H_0]. \end{aligned} \quad (\text{A16})$$

By using Eq.(A11), we then obtain

$$T(E) = t + \left[1 + t(E) \frac{1}{E - H_0}\right] t_w \left[1 + \frac{1}{E - H_0} t(E)\right]. \quad (\text{A17})$$

From the separable form Eq. (A2) for w , it is easy to find the solution of Eq. (A15)

$$t_w = \Gamma^\dagger \frac{1}{E - H_0 - \Sigma} \Gamma, \quad (\text{A18})$$

with

$$\Sigma = \Gamma \frac{1}{E - H_0 - v} \Gamma^\dagger \quad (\text{A19})$$

$$= \bar{\Gamma} \frac{1}{E - H_0} \Gamma^\dagger \quad (\text{A20})$$

$$= \Gamma \frac{1}{E - H_0} \bar{\Gamma}^\dagger, \quad (\text{A21})$$

where

$$\bar{\Gamma}^+ = [1 + t(E)\frac{1}{E - H_0}]\Gamma^+, \quad (\text{A22})$$

$$\bar{\Gamma} = \Gamma[1 + \frac{1}{E - H_0}t(E)]. \quad (\text{A23})$$

Substituting Eq. (A18) into Eq. (A17), we finally obtain

$$T(E) = t + \bar{\Gamma}^+ \frac{1}{E - H_0 - \Sigma} \bar{\Gamma}. \quad (\text{A24})$$

Taking the matrix elements of the relevant equations given above between the channels $a, b, c = \gamma N, \pi N, KY$ and noting that $H_0|N_i^* \rangle = M_{N_i^*}^0|N_i^* \rangle$ in the center of mass frame, $G_a = \langle a|\frac{1}{E-H_0}|a \rangle$, and $\Gamma_{N_i^*,a} = \langle N_i^*|\Gamma|a \rangle$, we then obtain Eqs. (1)-(6) in Section II A.

-
- [1] R. Bradford *et al.* [The CLAS Collaboration], Phys. Rev. C **73**, 035202 (2006); R.A. Schumacher, private communication (2005).
- [2] J. W. C. McNabb *et al.* [The CLAS Collaboration], Phys. Rev. C **69**, 042201 (2004); J.W.C. McNabb, PhD Thesis, Carnegie Mellon University (2002); R. Schumacher, private communication (2003).
- [3] K.H. Glander *et al.*, Eur. Phys. J. A **19**, 251 (2004).
- [4] R. Lawall *et al.*, Eur. Phys. J. A **24**, 275 (2005).
- [5] R. G. T. Zegers *et al.* [The LEPS Collaboration], Phys. Rev. Lett. **91**, 092001 (2003).
- [6] M. Sumihama *et al.* [The LEPS Collaboration], arXiv:hep-ex/0512053; M. Sumihama, private communication (2006).
- [7] J.C. David, C. Fayard, G. H. Lamot, and B. Saghai, Phys. Rev. C **53**, 2613 (1996); T. Mizutani, C. Fayard, G.H. Lamot, and B. Saghai, *ibid* **58**, 75 (1998).
- [8] T. Mart and C. Bennhold, Phys. Rev. C **61**, 012201 (2000).
- [9] B.S. Han, M.K. Cheoun, K.S. Kim, and I-T. Cheon, Nucl. Phys. **A691**, 713 (2001).
- [10] S. Janssen, D.G. Ireland, and J. Ryckebusch, Phys. Lett. B **562**, 51 (2003); S. Janssen, J. Ryckebusch, and T. Van Caueren, Phys. Rev. C **67**, 052201 (2003).
- [11] D.G. Ireland, S. Janssen, and J. Ryckebusch, Nucl. Phys. **A740**, 147 (2004).
- [12] P. Bydzovsky, M. Sotona, O. Hashimoto, and T. Takahashi, arXiv: nucl-th/0412035.
- [13] M. Guidal, J.-M. Laget, and M. Vanderhaeghen, Phys. Rev. C **68**, 058201 (2003).
- [14] T. Mart and C. Bennhold, arXiv: nucl-th/0412097.
- [15] T. Corthals, J. Ryckebusch, and T. Van Caueren, arXiv: nucl-th/0510056.
- [16] V. Shklyar, H. Lenske, and U. Mosel, Phys. Rev. C **72**, 015210 (2005); H. Lenske, V. Shklyar, and U. Mosel, arXiv: nucl-th/0512044.
- [17] A. Usov and O. Scholten, Phys. Rev. C **72**, 025205 (2005).
- [18] W.-T. Chiang, F. Tabakin, T.-S. H. Lee, and B. Saghai, Phys. Lett. B **517**, 101 (2001).
- [19] W.-T. Chiang, B. Saghai, F. Tabakin, and T.-S. H. Lee, Phys. Rev. C **69**, 065208 (2004).
- [20] B. Juliá-Díaz, B. Saghai, F. Tabakin, W. T. Chiang, T.-S. H. Lee, and Z. Li, Nucl. Phys. **A755**, 463 (2005).
- [21] B. Juliá-Díaz, B. Saghai, T.-S. H. Lee, and F. Tabakin, arXiv: nucl-th/0512010.

- [22] Z. Li and B. Saghai, Nucl. Phys. **A644**, 345 (1998).
- [23] B. Saghai and Z. Li, Eur. Phys. J. A **11**, 217 (2001).
- [24] B. Saghai, Proceeding of International Symposium on Electrophoto-production of Strangeness on Nucleons and Nuclei, Sendai, Japan (2003), Editors: K. Maeda, H. Tamura, S.N. Nakamura, and O. Hashimoto, World Scientific (2004), arXiv: nucl-th/0310025.
- [25] R. Koniuk and N. Isgur, Phys. Rev. Lett. **44**, 845 (1980); Phys. Rev. D **21**, 1868 (1980); Erratum *ibid* **23**, 818 (1981); S. Godfrey and N. Isgur, *ibid* **32**, 189 (1985); R. Koniuk and N. Isgur, Phys. Rev. Lett. **44**, 845 (1980).
- [26] S. Capstick and N. Isgur, Phys. Rev. D **34** 2809 (1986).
- [27] S. Capstick, Phys. Rev. D **46**, 2864 (1992).
- [28] S. Capstick and W. Roberts, Phys. Rev. D **49**, 4570 (1994).
- [29] S. Capstick and W. Roberts, Phys. Rev. D **58**, 074011 (1998).
- [30] S. Capstick and W. Roberts, Prog. Part. Nucl. Phys. **45**, 5241 (2000), and references therein.
- [31] R. Bijker, F. Iachello, and A. Leviatan, Ann. Phys. **236**, 69 (1994); *ibid* **284**, 89 (2000), and references therein.
- [32] M.M. Giannini, E. Santopinto, and A. Vassallo, Eur. Phys. J. A **12**, 447 (2001); Proceedings of NSTAR 2002 Workshop on the Physics of Excited Nucleons, Pittsburgh, PA (USA), 2002; Editors S.A. Dytman and E.S. Swanson, World Scientific (2003), arXiv: nucl-th/0302019.
- [33] T.-S. H. Lee, A. Matsuyama, and T. Sato, Proceeding of the Workshop on the Physics of Excited Nucleons, Grenoble, France, 2004; Editors J.-P. Bocquet, V. Kuznetsov, and D. Rebreyend, World Scientific (2004).
- [34] V. D. Burkert and T. S. H. Lee, Int. J. Mod. Phys. E **13**, 1035 (2004).
- [35] T. Sato and T.-S. H. Lee, Phys. Rev. C **54**, 2660 (1996); *ibid* C **63**, 055201 (2001).
- [36] K. Hagiwara *et al.*, Particle Data Group, Phys. Rev. D **66**, 010001 (2002).
- [37] R.A. Arndt, W.J. Brisco, I.I. Strakovsky, and R.L. Workman, Phys. Rev. C **66**, 055213 (2002); <http://gwdac.phy.gwu.edu>.
- [38] S. Kamalov and S.N. Yang, Phys. Rev. Lett. **83**, 4494 (1999).
- [39] Z. Li and R. Workman, Phys. Rev. C **53**, R549 (1996).
- [40] B. Saghai and Z. Li, Proceedings of NSTAR 2002 Workshop on the Physics of Excited Nucleons, Pittsburgh, PA (USA), 2002; Editors S.A. Dytman and E.S. Swanson, World Scientific (2003), arXiv: nucl-th/0305004.

- [41] A. Švarc and S. Ceci, arXiv: nucl-th/0009024.
- [42] W.-T. Chiang, S.N. Yang, L. Tiator, M. Vanderhaeghen, and D. Drechsel, Phys. Rev. C **68**, 045202 (2003).
- [43] G.-Y Chen, S. Kamalov, S.N. Yang, D. Drechsel, and L. Tiator Nucl. Phys. **A723**, 447 (2003).
- [44] V. A. Tryasuchev, Eur. Phys. J. A **22**, 97 (2004).
- [45] J.-Z. Bai *et al.* (BES Collaboration), Phys. Lett. B **510**, 75 (2001).
- [46] M. Ablikim *et al.* (BES Collaboration), arXiv: hep-ex/0405030; B.S. Zou (BES Collaboration), Proceeding of the Workshop on the Physics of Excited Nucleons, Grenoble, France, 2004; Editors J.-P. Bocquet, V. Kuznetsov, and D. Rebreyend, World Scientific (2004); Sh. Fang (BES Collaboration), arXiv: hep-ex/0509034.
- [47] N.G. Kelkar, M. Nowakowski, K.P. Khemchandani, and S.R. Jain, Nucl. Phys. **A730**, 121 (2004).
- [48] M. L. Goldberger and K. M. Watson, *Collision Theory*, Robert E. Krieger Publishing Company (1975).
- [49] D. Dutta, H. Gao, and T. S. H. Lee, Phys. Rev. C **65**, 044619 (2002).
- [50] A. Manohar and H. Georgi, Nucl. Phys. B **234**, 189 (1984).
- [51] Z. Li, H. Ye, and M. Lu, Phys. Rev. C **56**, 1099 (1997).
- [52] N. Isgur and G. Karl, Phys. Lett. B **72**, 109 (1977); N. Isgur, G. Karl, and R. Koniuk, Phys. Rev. Lett. **41**, 1269 (1978); J. Chimza and G. Karl, Phys. Rev. D **68** 054007 (2003).
- [53] R.D. Baker *et al.*, Nucl. Phys. **B141**, 29 (1978).
- [54] R.D. Baker *et al.*, Nucl. Phys. **B145**, 402 (1978).
- [55] T.M. Knasel *et al.*, Phys. Rev. D **11**, 1 (1975).
- [56] D.H. Saxon *et al.*, Nucl. Phys. **B162**, 522 (1980).
- [57] J.C. Hart *et al.*, Nucl. Phys. **B166**, 73 (1980).
- [58] I.G. Alekseev *et al.* (EPECUR and ITEP-PNPI Collaborations), arXiv: hep-ex/0509032.
- [59] *see e.g.* J. Imazato, Nucl. Phys. Proc. Suppl. **129**, 81 (2004).
- [60] B. Saghai, Proceeding of the Workshop on the Physics of Excited Nucleons, Grenoble, France, 2004; Editors J.-P. Bocquet, V. Kuznetsov, and D. Rebreyend, World Scientific (2004), arXiv: nucl-th/0408054.
- [61] K.H. Althoff *et al.*, Nucl. Phys. **B137**, 269 (1978).
- [62] R.A. Adelseck and B. Saghai, Phys. Rev. C **42**, 108 (1990); I.J. General and S.R. Cotanch,

- Phys. Rev. C **69**, 035202 (2004).
- [63] U. Thoma, arXiv: nucl-ex/0501007.
- [64] M.Q. Tran *et al.* (The SAPHIR Collaboration), Phys. Lett. B **445**, 20 (1998).
- [65] B. Saghai, Proceeding of International Symposium on Hadrons and Nuclei, Seoul, Korea (2001), Editors: I.-T. Cheon, T. Choi, S.W. Hong, and S.H. Lee, AIP, Vol. 594 (2001), arXiv: nucl-th/0105001.
- [66] T. Mart, A. Sulaksono, and C. Bennhold, arXiv: nucl-th/0411035.
- [67] A.V. Anisovich, A. Sarantsev, O. Bartholomy, E. Klempt, V.A. Nikonov, and U. Thoma, Eur. Phys. J. A **25**, 427 (2005); A.V. Sarantsev, V.A. Nikonov, A.V. Anisovich, E. Klempt, and U. Thoma, Eur. Phys. J. A **25**, 441 (2005).
- [68] O. Bartholomy *et al.*, Phys. Rev. Lett. **94**, 012003 (2005).
- [69] R. Bradford and R. Schumacher, arXiv: nucl-ex/0602004.